Spring 2021

Kinetics Studies on Isomerization and Unimolecular Decay Processes of the Criegee Intermediate, Methacrolein (MACR) Oxide

Hyun Kyung Lee , '21

Kinetics Studies on Isomerization and Unimolecular Decay Processes of the Criegee Intermediate, Methacrolein (MACR) Oxide

Hyun Kyung Lee

Swarthmore College

Department of Chemistry and Biochemistry

April 2021

Acknowledgments

I would like to thank all my friends and family for support. I would have not been able to finish this thesis without any of them. I am also immensely thankful for Professor Tom Stephenson and his immense kindness and patience while I was trying to figure out all the new computational methods. I would also like to thank Swarthmore College for all the funding that made this research possible.

Abstract

Alkenes are one of the major components of hydrocarbons in our atmosphere. One of the most common alkenes in our atmosphere is isoprene (2-methyl – 1,3 – butadiene). Currently, it is known that isoprene ozonolysis can lead to the production of Criegee intermediates CH_2OO, methacrolein (MACR) oxide, and methyl vinyl ketone (MVK) oxide. In part, we were interested in studying one specific Criegee intermediate, MACR oxide. The competition between the isomerization reactions and the unimolecular reactions became the focus of our study. Rate constants for the relevant reactions were calculated by implementing RRKM theory and using Master Equation modeling to create a scheme for the system. The overall results show that the most favorable reaction of MACR oxide is the isomerization between the cis and trans conformations. Because the transition states between these conformations are relatively low compared to the other transition states in the reaction, the conversions are observed to happen much faster than the others. The next fastest reaction that takes place is the unimolecular decay reactions to the dioxiranes and the dioxole. The decay reactions involved barriers that were higher than the cis⇌trans conversion but still lower than the barrier between the anti⇌syn conversion. With dioxole being our most stable state, our main interest was if different conformers of MACR oxide will decay to this structure in an atmospherically relevant time frame. It was found that substantial fraction (80%) of MACR oxide cannot decompose to dioxole in the relevant time frame as the barrier for the conversion between anti and syn is too high. We saw that there was almost no anti⇌syn conversion in any of our calculations.

Table of Contents

Chapter 1: Introduction

Alkenes are one of the major components of hydrocarbons in our atmosphere. One of the most common alkenes in our atmosphere is isoprene (2-methyl – 1,3 – butadiene), with an annual global emission of 500 Tg per year.[1] In a prior study done by Sindelarova et al in 2014, it was observe isoprene constituted 70% of the population that out of the mean annual emission of 760 Tg of biogenic volatile organic compounds.[2] Because isoprene is found in such abundant amounts, it is important to know how this compound could go through different reactions and affect atmospheric chemistry.

It is well known that isoprene can be removed from the atmosphere through oxidation reactions with hydroxyl radicals (OH), ozone (O_3), and nitrate radicals (NO_3).[3] O_3 oxidizes alkenes, including isoprene, in a reaction known as ozonolysis. In the atmosphere, this reaction is often the source of OH radicals which becomes important as OH can react with many pollutants in the air and reduce the number of greenhouse gases, such as methane or O_3 in our atmosphere.[1] OH also reacts with volatile organic compounds to produce organic peroxy radicals. These radicals can go through a reaction to produce NO and NO_2, a critical process in making of the ozone in the troposphere.[4] Through the UK TORCH Campaign in 2003, it has been noted that 43% of OH was produced through the reaction of an alkene with O_3 during a particular heatwave period.[5] Because atmospherically important chemical reactions also happen not only in the daylight hours but also during the night, it is of interest to see if the production of OH differs depending on whether the sun is shining or not. From an earlier study, we know that the nighttime production of OH is entirely dominated by ozonolysis .[6] Because OH helps determine our air quality, it is important to understand how these radicals are

formed. It is therefore important to understand the complexity of the ozonolysis reaction including its energetics, intermediates, and products.

1.1 Criegee Intermediates

Rudolf Criegee was the first to propose that the ozonolysis of the alkenes proceeds via a 1,3-cycloaddition across the double bond to form a primary ozonide. Due its high instability, the molecule then decomposes into a carbonyl compound and a carbonyl oxide, a Criegee intermediate (**Scheme 1**).[7,8] This molecule is the key intermediate in the ozonolysis process. Depending on the internal energy distribution of primary ozonide, different Criegee intermediates can be formed. Those that are formed with low thermal energies are called stabilized Criegee intermediates while those with very high internal energies are called chemically activated Criegee intermediates.[9]

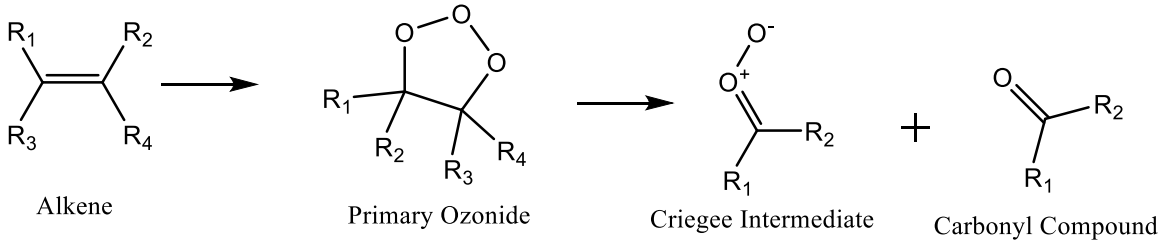

Scheme 1. Alkene ozonolysis proceeding through primary ozonide to Criegee intermediate and carbonyl compounds

Criegee intermediates then can either promptly undergo unimolecular decay into OH radicals (via internal hydrogen transfer reactions), collisional stabilization (for example, with inert atmospheric gases such as N_2), or bimolecular reaction with trace species in the atmosphere (e.g. water vapor, SO_2, NO_2, and acids).[10] When highly energized Criegee intermediates go through unimolecular decay, OH and other products

are rapidly formed. Stabilized Criegee intermediates go through thermal unimolecular decay to form OH or other products such as dioxole and dioxirane.[1] Most of the OH from isoprene ozonolysis is suspected to be produced from the Criegee intermediate called methyl vinyl ketone (MVK) oxide, described below.[11]

Currently, it is predicted that isoprene ozonolysis can lead to the production of Criegee intermediates CH_2OO, methacrolein (MACR) oxide, methyl vinyl ketone (MVK) oxide (**Scheme 2**). The first direct evidence of gas phase Criegee intermediate was observed by Taatjes et al. in 2008. They were able to observe formaldehyde oxide (CH_2OO) in the gas phase by using photoionization.[12] With now the knowledge of direct observation of the Criegee intermediate, Welz et al. then studied direct kinetics of the formation of the Criegee intermediate formaldehyde oxide (CH_2OO) from the reaction of CH_2I with O_2.[13] Direct observation of different Criegee intermediates were also starting to be studied. In particular, Beames et al. was able to examine the photochemistry of the alkyl-substituted Criegee intermediate CH_3CHOO and studied its analogous properties with that of CH_2OO using UV absorption spectroscopy.[14]

As the data for the experimental observations were starting to increase, scientists started to compare computational values to those of the experimental values. Lester and Klippenstein focused on looking at how the values for the structures and kinetics derived from computational methods compared to those observed by the experimental measurements for the Criegee intermediate $(CH_3)_2COO$.[10] Their study showed that the predicted rate constants of the unimolecular decay were 276 s^{-1} at 298 K while the experimentally measured values were 361 ± 49 s^{-1} at 298 K. It was therefore shown that the calculated values match well to those of experimentally measured values indicative of

the good accuracy of the highly theoretical calculation methods. A more recent review done by Taatjes looks at the direct observation of Criegee intermediates and their reaction kinetics for novel reaction paths followed by these molecules. These include cycloaddition reactions, unimolecular reactions, and insertion reactions. The experimental values were then compared to those of the theoretical values.[15] With the increasing amount of comparison between the calculated and the measured values, knowledge about Criegee intermediate reactivity is currently still being extended.

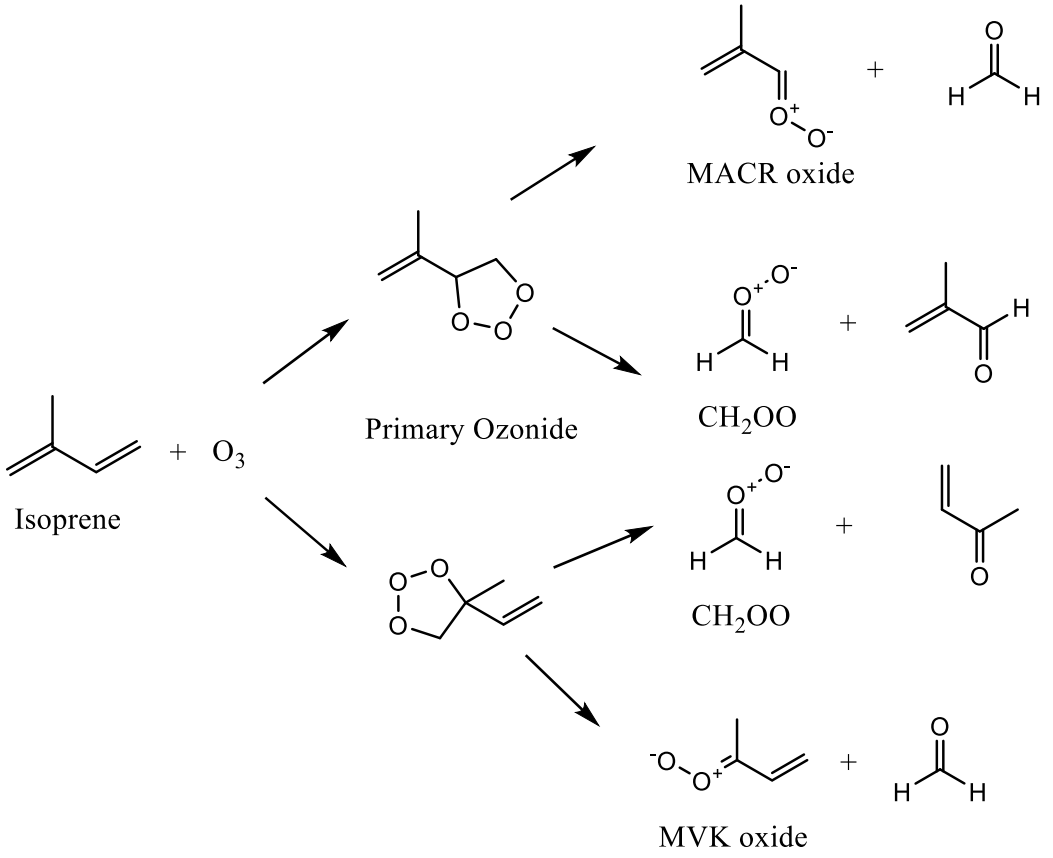

Scheme 2. Ozonolysis of isoprene producing CH2OO, MACR oxide, and MVK oxide.[16] Modified from ref 16.

As shown in **Scheme 2**, the cycloaddition of ozone across one of the C, C double bonds leads to two distinct primary ozonides which then can decompose into the products

mentioned above.[16] The overall production of each intermediate is estimated to be 58% CH_2OO, 23% MVK oxide, and 19% MACR oxide. Among these Criegee intermediates, MVK oxide and MACR oxide can undergo ring closure to create dioxirane or H-migration to form a hydroperoxide intermediate. The hydroperoxide is then predicted to decompose to form OH and RCO radicals.[4] A third rearrangement that can occur is the rapid electrocyclic ring closure which leads to the formation of dioxole -a five-membered cyclic peroxide. However, this mechanism only occurs for Criegee intermediates that have the terminal oxygen oriented towards the vinyl group (**Scheme 3**).[17] The rate and the mechanism of the unimolecular reactions of MVK and MACR oxide are predicted to be very different from each other and dependent on their conformational form. Past theoretical studies indicate that these two Criegee intermediates proceed with distinct paths depending on the thermal conditions.[17]

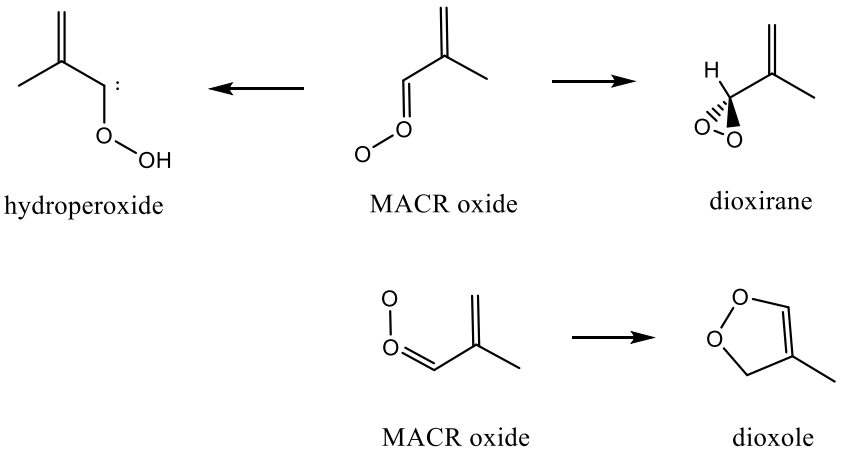

Scheme 3. An example of the formation of hydroperoxide, dioxirane, and dioxole structures from corresponding Criegee intermediates.

Although there has been a significant amount of research done on CH_2OO, MVK oxide, and MACR oxide there are still unresolved issues. Presently, MVK oxide and MACR oxide are predicted to undergo different unimolecular decay processes and biomolecular reactions to produce various products, some of which lead to aerosols that affect the climate. Depending on the rate constants of both unimolecular and the bimolecular processes, the Criegee intermediates are expected to go through different atmospheric reactions and thus affect the atmospheric chemistry in different ways.[3]

To date, there have been theoretical calculations completed studying MVK oxide and MACR oxide formation pathways and their reactions.[4,16] These calculations help in predicting the fates of each of the intermediates. Along with the theoretical calculations, Vansco et al. have been successful at finding experimental evidence for the formation of dioxole from these intermediates. The finding of this process further strengthens the proposed mechanism of the unimolecular decay to the dioxole.[17] However as noted by Vansco et al, since there is still very little known about both MVK oxide and MACR oxide, it is important to see how these two intermediates behave in the atmosphere.

For MVK oxide, we know that one pathway yields OH through the 1,4-H atom transfer while another pathway form dioxole through a rapid electrocyclic ring closure. MACR oxide on the other hand does not have a 1,4-H atom transfer pathway available. Instead depending on its starting conformation, it can either go through a slow ring closure of the carbonyl oxide group to form dioxirane or produces dioxole via rapid ring closure. [3] Our main goal of the study is to study these pathways in MACR oxides and try to see what types of competition exist between the reaction pathways and find out how they affect atmospheric chemistry.

1.2 Unimolecular Reactions

In this work, we are focused on the unimolecular reactions of Criegee intermediates. Typically, unimolecular reactions are represented as

$$A^* \rightarrow Products \quad (1)$$

Where A* is a molecule with enough activation energy to generate products.[18] For the Criegee intermediates, sufficient energy is proposed to be gained through the collision with the inert atmospheric gases such as nitrogen and then transform into its products.

The unimolecular reactions that we are interested in for our study are the isomerization reactions. The energy profile for these types of reactions includes a substantial potential energy barrier separating the two isomers (**Figure 1**).

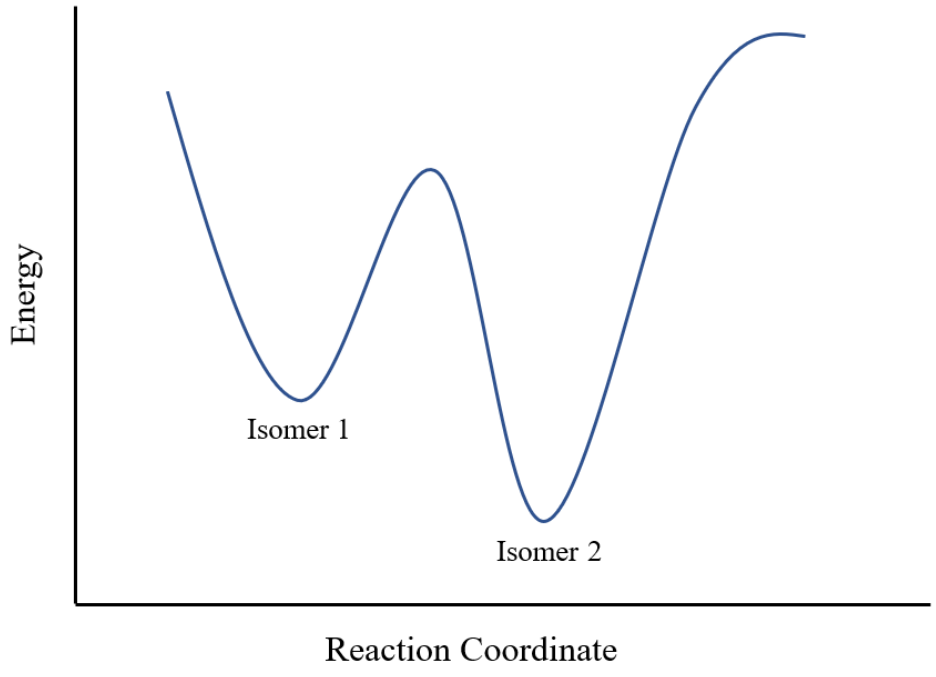

Figure 1. Energy profile for the isomerization reaction.

To further understand the unimolecular reactions, it is important to investigate the rate of the chemical reaction and the dependence of this rate on environmental factors such as temperature and pressure.[19] Having an understanding of the rate constants allows us to see the necessary dynamics of the unimolecular reactions.

To explore the unimolecular reactions and find the corresponding rate constants, we have taken the following steps:

1. Calculate the energies of all products, reactants, and transition states;
2. Apply a model, Rice-Ramsperger-Kassel-Marcus (RRKM) theory, to determine energy-resolved rate constants, k(E), that connect the reactants and products;
3. Use Master Equation Modeling to implement all of the above, incorporating a scheme for collisional activation and the Boltzmann distribution, resulting in thermally averaged rate constants, k(T), for the parallel and competing rate processes.

1.3 Molecular Geometry and RRKM theory

The calculations of the energies of products, reactants, and transition states were conducted by using Gaussian software. Because the input of the molecular geometry becomes important in steps 2 and 3, the correct calculations of the optimized structures become essential to the study. Once the geometry has been optimized, we start to apply the RRKM theory. Using this theory, we can find the rate coefficients for unimolecular decay. When paired with the high-level electronic structure theory, the RRKM theory is shown to be a robust tool for understanding unimolecular reactions.[1] This theory is a statistical unimolecular rate theory. The isomerization or dissociation of A* is represented as:

$$A^* \xrightarrow{k(E)} A^{\ddagger} \longrightarrow \text{Products} \quad (2)$$

where $A^{\ddagger}$ is the transition state.[18] The theory runs under an important assumption that a molecule prepared with the energy of E populates all of the possible states statistically and maintains a uniform distribution during the decay.

The energy-dependent RRKM rate constants are expressed as[20]

$$k(E) = \frac{W(E-E_0)}{h\rho(E)} \quad (3)$$

where $W(E-E_0)$ is the rovibrational sum of states at the optimized transition state geometry, E_0 is the reaction threshold energy, h is Planck's constant, and $\rho(E)$ is the density of rovibrational states of the reactants. Accurate knowledge of the electronic structures and the vibrational and rotational characteristics of the molecule is important to derive the sum of the states and the density of states.[18] These structures and calculations are obtained through high-level electronic structure theory used in Gaussian.

1.4 Master Equation Modeling

Unimolecular reactions such as those of the Criegee intermediates cannot be described using solely thermodynamic equilibrium. Because in this kind of chemical reaction there is competition between the kinetic time scale and thermalization time scale, an appropriate model that can treat this competition needs to be applied. Currently, master equation (ME) modeling is considered to be successful at implementing this system. A ME model is a set of a coupled linear differential equations that describe both the energy transfer and chemical transformation that occurs on a potential energy surface. A representative potential energy surface is shown in **Scheme 4**, where it has two local minima representing the metastable species that in theory can be isolated. The wells are

connected by a transition state which allows the conversion from one isomer to another. The energy of the transition state represents the energy barrier for the reaction. Energy activation or deactivation for gas-phase molecules happens through collision and leads to molecules achieving different degrees of excitation.[20]

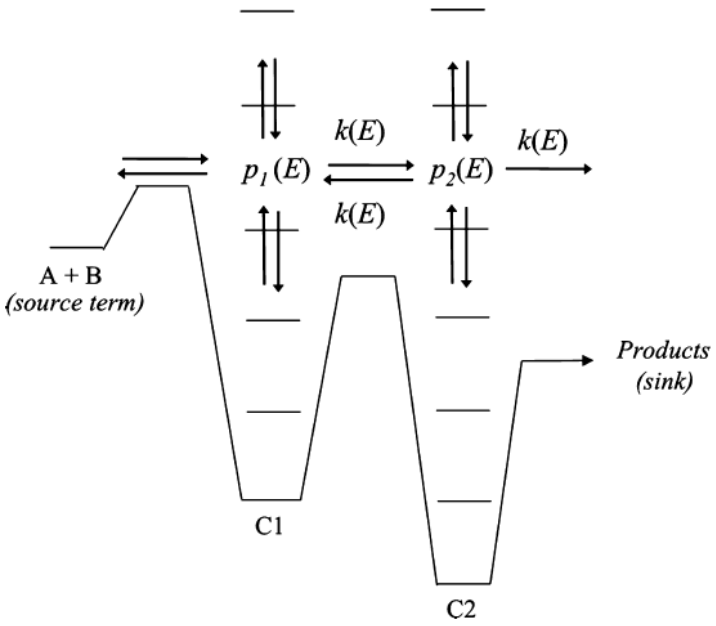

Scheme 4. Potential energy surface of a gas-phase unimolecular system with two wells[20]. Adapted from ref 20.

To successfully implement the ME method, first mechanistic pathways must be documented. This involves the completion of the first two steps mentioned previously:

1. The calculation and search for the reactants, intermediates, transition states, and products using the appropriate electronic structure methods implemented in Gaussian.
2. Calculation of rate constants k(E) using RRKM theory.

There are two ways in which rate constants can be measure: k(E) and k(T). The kinetic quantity k(E) is appropriate for use when the energy of the system is well-defined. It is characterized by specific energy. However, for atmospheric chemistry, it makes sense to measure the relevant kinetics by k(T) which is the rate constant defined at a specific temperature.[1] In the atmosphere, depending on the altitude the temperature changes. By using k(T), we can then model this change in the environment. ME modeling has been shown to successfully describe reaction systems using phenomenological, thermal rate coefficients k(T) for coupled reactions in the complicated scenarios that appear in combustion or atmospheric chemistry.[21]

To derive k(T), the equation below can be used[1]:

$$k(T) = \int_{E_0}^{\infty} k(E)P(E,T)dE \quad (4)$$

Where E_0 is the activation energy and P(E, T) is the distribution of internal energies at temperature, T. As seen in the equation, k(T) and k(E) are related to each other. Due to the connection between the two, it is important to obtain detailed information about k(E) to determine the correct k(T). The more we know about the k(E) through the implementation of RRKM theory, the more accurate k(T) becomes. After calculating these constants, collisional energy transfer also needs to be characterized. The transfer of energy is characterized by choosing a probability function that describes the probability of collision changing the internal energy of the molecule.

Once the previous two steps have been implemented, the ME then can be solved by matrix diagonalization. Solving ME by matrix diagonalization allows for concentration versus time profiles of configurations to be observed along with phenomenological rate coefficients, k(T)[21]. This matrix diagonalization is solved using a

program called a Master Equation Solver for Multi-Energy Well Reactions (MESMER). MESMER provides a general and flexible program to facilitate solving of ME for different unimolecular systems with an arbitrary number of wells, transition states, reactants, and products.[20]

Chapter 2: Methods

2.1 General Outline

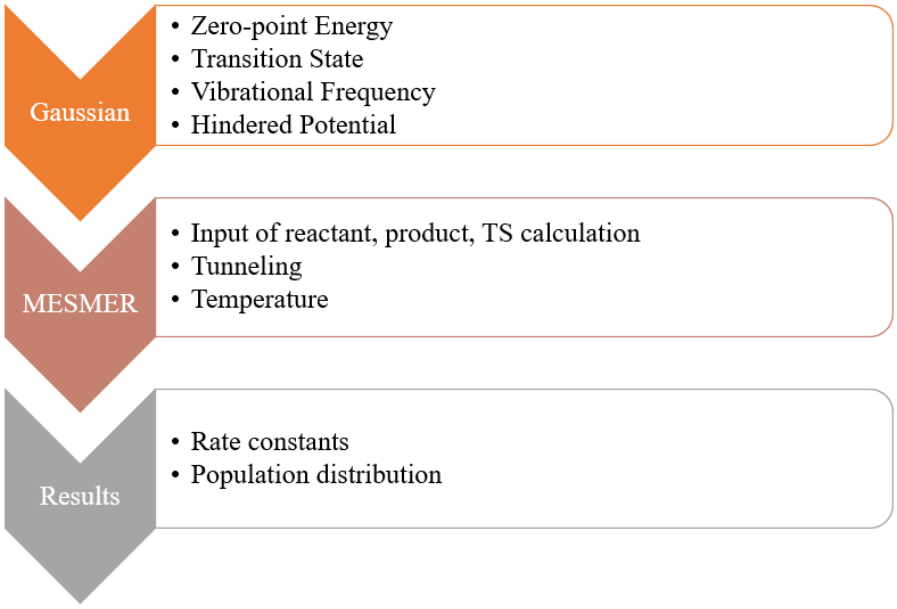

Scheme 5. A general outline of calculation steps. The content in the box is what we try to find in each step.

The calculation steps follow the general scheme above. The optimal molecular geometries of the reactants, products, and transition states are first found using Gaussian. Then we input the data of the compounds and other environmental factors into MESMER to calculate rate constants and population distribution of the compounds.

2.2 Gaussian Calculations

All calculations were done with Gaussian 16. The program was used to find the appropriate zero-point corrected energies of the molecules along with their vibrational frequencies, rotational constants, and torsional potentials. The following methods and basis sets were used: B3LYP/cc-pVTZ and B2PLYPD3/cc-pVTZ. To choose the best

methods and basis sets, preliminary calculations were conducted by Rory Schmidt in the summer of 2020.

2.2.1 Basis Sets

Before starting a quantum mechanical calculation, it is important to decide which basis set to use. A basis set allows for the approximation of a molecule's wave function and depending on the size and the composition of the basis set the accuracy changes. The sizes of these sets usually range between the minimal number required to contain an atom's electrons and the several energy levels higher. In our studies, we employed a basis set cc-pV*n*Z (where *n* ranges from 2 to 6) that was developed by Dunning and his co-workers.

To test which size of the basis set allows for the most efficient calculations, different sizes were tested for cc-pV*n*Z where *n* could be double (D), triple (T), quadruple (Q), and quintuple (5). For D and T, augmented versions were attempted to see if there were any improvements in accuracy. By looking at the non-zero-point corrected energies of the anti-trans-MACR molecule, we could compare the results of the basis sets to each other. The results show that with the increasing basis set size, we do see an improvement in energy calculation. However, as the basis set was increased to the quadruple basis set, we see that the computational cost start to increase greatly (**Table 1** and **Figure 2**). The timescale of calculations increased from the minutes to hours and upon applying the quintuple basis set, the calculation did not converge even after running for about a week.

Table 1. Comparison of computation time, energy, and basis set for optimization of the anti-trans MACR oxide Criegee intermediate. B3LYP functional was used with cc-pV*Z basis set where * = D, T, Q, or 5. Data collected by Rory Schmidt in 2020.

Basis set	Energy (Hartrees)	CPU time (hours:min: sec)
Double (D)	-306.3308	00:14:34
Aug-double (D)	-306.3613	00:30:18
Triple (T)	-306.4340	00:58:37
Aug-triple (T)	-306.4401	05:58:27
Quad (Q)	-306.4594	14:54:04
Quint (5)	-306.4674	≈ 1 week

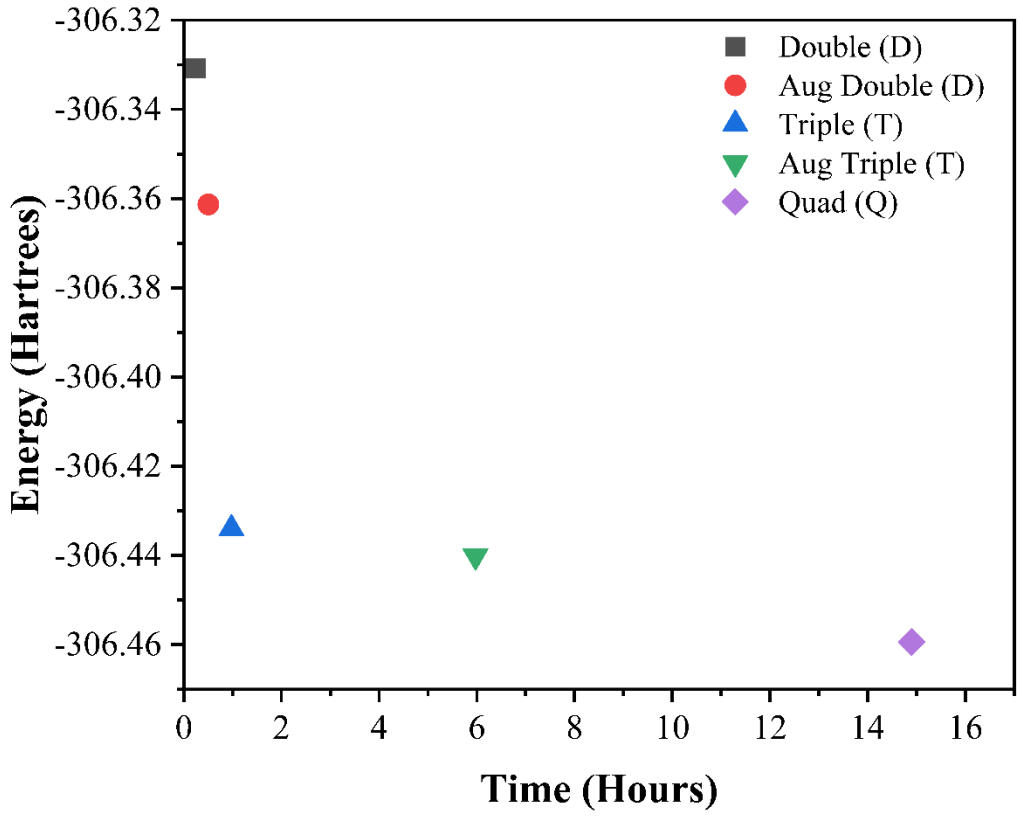

Figure 2. Comparison of computation time, energy, and basis set for optimization of the anti-trans MACR oxide Criegee intermediate. The data for the quintuple basis sets was not denoted on the graph due to the skewing of the data.

The application of the augmented basis sets was not tested after the triple zeta basis sets as we saw that there was not much improvement in calculations while there was an increase in CPU time. Since computing time increased considerably after the cc-pVTZ basis set, we decided to move forward with the triple basis set as it provided us with the best balance between cost and accuracy.

2.2.2 Density functional Methods

The next computational choice that had to be made was the density functional method to be used. The following five functional methods were tested: B2PLYP, B2PLYPD3, B3LYP, B3LYPD3, and MN12L. In a study conducted by Smith and Karton, it was noted that on average, the MN12L functional method gave the best balance for calculations on a set of Criegee intermediates.[22] (This set did not include the molecules that are under examination here.) However, Grimme and Steinmetz report that B2PLYP is also successful at calculating energies and the molecular geometries of a wide range of organic compounds.

Table 2. Difference in energy for each conformation between the functional methods and the literature value computed through high-level Coupled Cluster Method (CCSD-CBS).[3]

Method	Anti-cis (kcal/mol)	Syn-trans (kcal/mol)	Syn-cis (kcal/mol)	Average (kcal/mol)
B2PLYP	0.280	0.087	-0.079	0.15
B2PLYPD3	0.305	-0.094	-0.238	0.21
B3LYP	0.266	0.257	0.473	0.33
B3LYPD3	0.311	-0.237	0.117	0.22
MN12L	0.830	-0.412	1.080	0.77

Table 3. Computational time taken for each functional method for the respective MACR Oxide conformers.

Methods	Anti-cis time (s)	Syn-trans time (s)	Syn-cis time (s)	Syn-trans time (s)
B2PLYP	29717.6	28947	30935	31799.2
B2PLYP-D3	30842	30355	30115.1	30943.4
B3LYP	2388	2390	2525	2515
B3LYP-D3	2378	2395	2537	2454
MN12L	3080.4	3101	3281	3289

The addition of dispersion correction to the functional method further improved the results of the calculations. If higher accuracy was needed for the structures, B2PLYP-D3 was recommended.[23]

To see if these functional methods also worked for our Criegee intermediate, MACR oxide, and its derivatives, we ran calculations using these five methods and compared their calculations. To test for the accuracy of the calculation methods, energy of anti-cis, syn-cis, and syn-trans MACR oxides were found relative to the most stable isomer, the anti-trans conformation. The structures of these confirmations will be explained in more detail later in the results sections. For now, the important part is that the energy of these structures was compared to those of the literature data which were computed through a high-level Coupled Cluster method (CCSD-CBS) (**Table S1**). The results show that MN12L was the least accurate method while B2PLYP gave the smallest amount of difference in energy with the literature values in its calculation showing superiorit (**Table 2**)

. However, we also see that B3LYP gave an error comparable to B2PLYP given that its computational time is much smaller than those of B2PLYP (**Table 3**). Because of these observations, we decided to do our preliminary calculations of the structure with B3LYP as it had the cheapest cost with a reasonable result. Because we were concerned about accounting for non-bonding interaction and dispersion of the hindered motions the molecules, we then decided to use B2PLYP-D3 for our refinement calculations. The addition of dispersion correction did not increase the computational time but also had advantages such as high accuracy as well as high consistency of the structures with only 0.3 - 0.4% deviation.[24]

2.3 Implementation of RRKM Theory

After the molecular geometries of the structures were calculated using Gaussian, RRKM theory was implemented to find energy-dependent rate constants k(E) that connects between the reactants and the products. As briefly mentioned in the introduction finding k(E) through RRKM theory will ultimately help us determine the temperature-dependent rate constant k(T) through the relationship represented by **equation 4**. One sensitive part of RRKM theory is how the density of rotational and vibrational states are calculated. The value of the density of states depends on many inputs such as the reactant's total energy, angular momentum, moments of inertia, and harmonic vibrational frequencies. For our study, although we have a good idea for the energy levels of all compounds, the ambiguity comes in with how to treat low vibrational frequencies that more closely resemble intramolecular torsions. Depending on how we treat such motions, the results of the RRKM theory could drastically change, thus it was important to decide

whether we would like to treat them as a harmonic vibrational frequency or hindered rotors.

2.3.1 Hindered Rotor Potential

One important aspect of our research revolves around finding the potential rotors of our compounds. As we already know, molecules can have rotational energy along with their transitional, and vibrational energies. In the four MACR oxide conformers and each of their transition state, two potential rotors can be found: hindered methyl rotors and rotors corresponding to motion about the C-C central bond. These two rotors contribute greatly to the vibrational density of states of the molecules because of their low frequency and thus need to be considered carefully when studying the reaction. Because the two rotors were considerably floppy, we inferred that it would not be wise to treat them as low vibration harmonic frequency as this could skew the outputs of the RRKM theory. Instead, we suspected that treating them as hindered rotors give us more accurate calculations.

2.3.2 Hindered rotor potential of Methyl Rotors

To implement the hindered rotor potentials for the methyl groups we first calculated the hindered potential of methyl rotors in the structures in Gaussian. Because the hindered rotor potentials were perfectly symmetrical, it was possible to simply graph the potential to a graphing software, Igor 8, and fit to a Fourier cosine expansion function below:

$$f(\theta) = b_0 + b_1 \cos\left(\theta\left(\frac{\pi}{180}\right)\right) + b_2 \cos\left(\theta\left(\frac{\pi}{180}\right)\right) + \cdots + b_n \cos\left(\theta\left(\frac{\pi}{180}\right)\right) \quad (5)$$

From the fit, we were then able to obtain coefficients that were needed as an input into MESMER for its analytical method of hindered rotor analysis. The fits of the methyl

rotor were all quite fitted well as shown by the supplemental figures (**Figures S1-S13**). The coefficients that were obtained through the fit are listed in **Table S2-S4.**

2.3.3 Hindered rotor potential for C-C central bond

The C-C central bond rotor was treated the same way as the methyl rotors but had a different implementation process into MESMER. The same potential calculations were run on Gaussian. However, due to some uncertainty in how to treat the angle phases for the asymmetric plot of the C-C rotors, we decided that it would be better to allow the MESMER software to do a fit to the calculated potential. This process then would let MESMER translate the potentials into energy levels of the Hamiltonian that is equivalent to that of the low vibrational frequency and allow for the implementation of the RRKM theory. MESMER allows for an input of the data of the hindered rotor potential and processes a fitting for that potential by using cosine and sine functions. However, we noticed that the fits for the C-C central bond rotors given from MESMER did not match up well to the calculated values from Gaussian as shown in **Figure 3**. More examples of the failed fits are shown in supplemental figures (**Figures S14-S22**). Many attempts were tried to figure out what was wrong, but because of time constraints, the investigation of this problem was not continued, and instead, the calculations were run without accounting for the central hindered potentials.

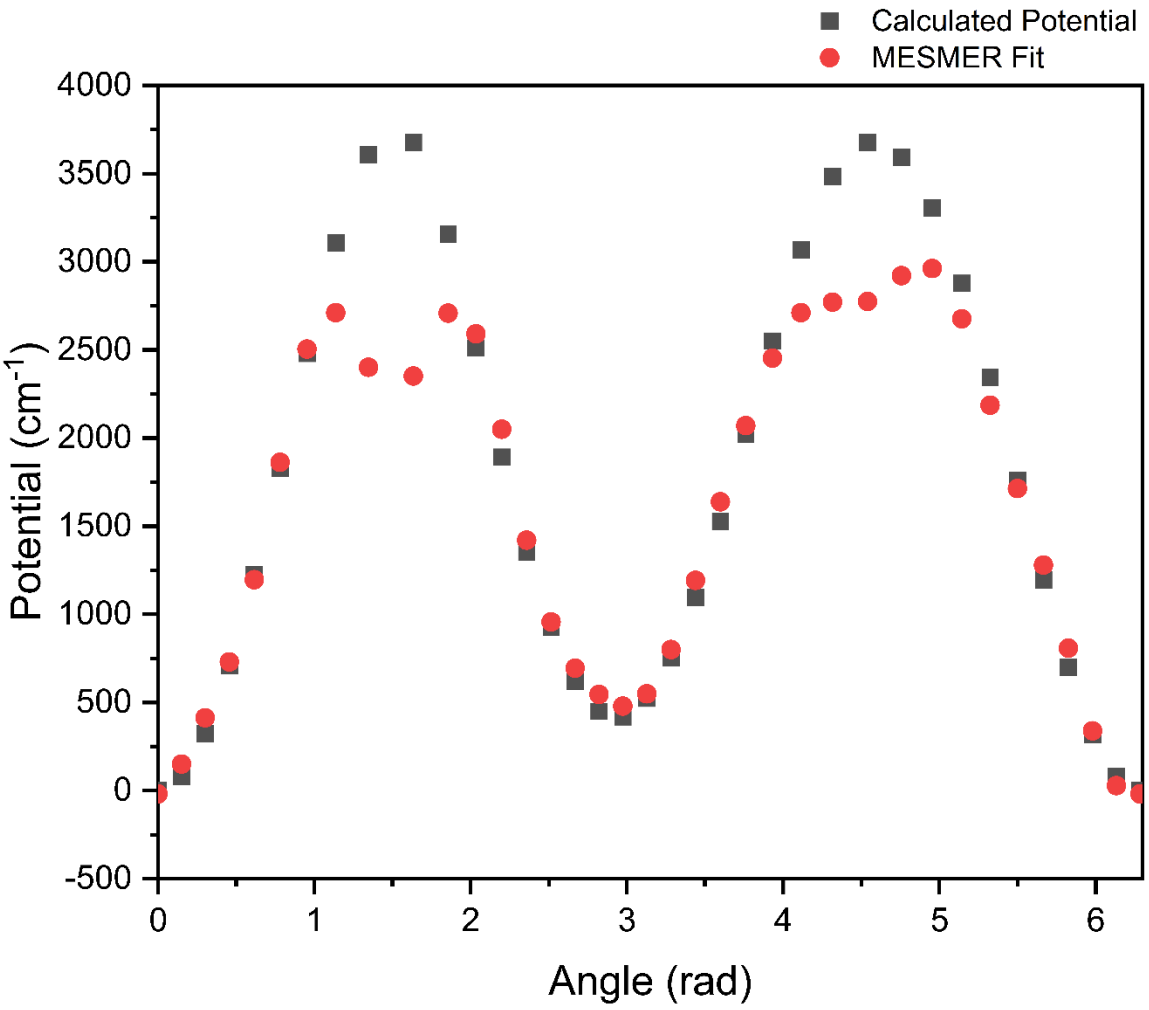

Figure 3. Graph of the calculated potential of anti-trans to trans-dioxirane TS vs. Mesmer fit.

2.4 Master Equation Solver for Multi-Energy Well Reactions (MESMER)

All rate constants and populations of the species were determined through an open-source software called MESMER. The program applies matrix techniques to solve the ME for systems that are composed of an arbitrary number of wells, transition states, sinks, and reactants.[20] Various inputs could be added to the system so that the reaction

could be simulated under different situations. For our study, we were also considered the effects of tunneling and temperature.

Chapter 3: Results and Discussion

3.1 MACR Oxide four major isomers and their transition states (TS)

3.1.1 Optimization of Molecular Geometry

MACR oxide exists as four major conformers: anti-trans, anti-cis, syn-cis, and syn-trans (**Scheme 6**). The optimized geometry of each conformer and the transition states that connect them were first found using the more efficient B3LYP functional with a cc-pVTZ basis set, and then optimized using more sophisticated B2LYPD3/cc-pVTZ calculations.

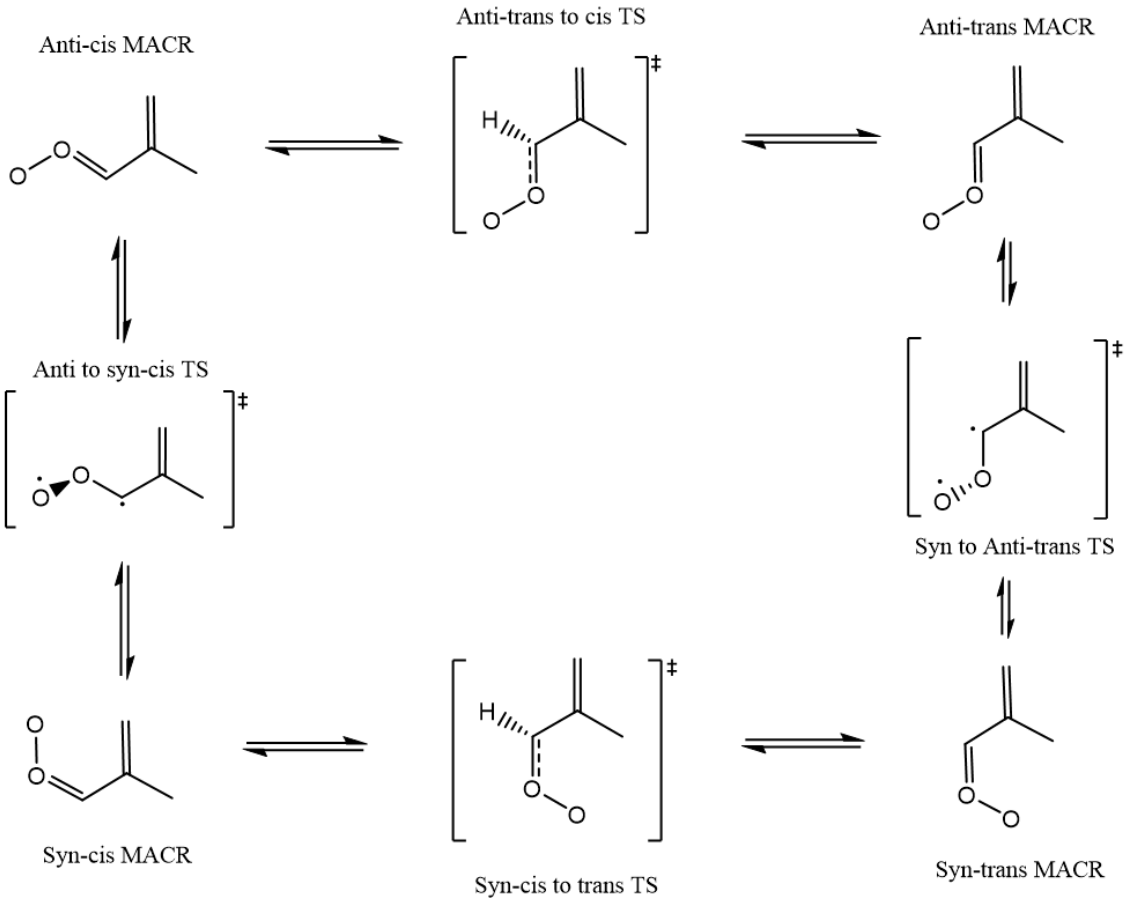

Scheme 6. Four conformers of MACR oxide and their isomerization pathways.

Out of all isomers possible in this pathway, anti-trans MACR oxide is observed to have the lowest energy (including zero-point corrections). The energies of all the other structures are tabulated relative to this specific isomer. **Table 4** below lists the energies of the four conformers along with the various transition states.

Table 4. Relative energies of the MACR oxide four conformers and their transition states compared to anti-trans MACR oxide. The energies were calculated using B2PLYPD3/cc-pVTZ.

MACR Oxide structures	Calculated energy (kcal/mol)	Literature value Energy[16] (kcal/mol)
Anti-trans	0.00	0.0
Anti-trans to anti-cis TS	10.08	8.6
Anti-cis	3.49	3.2
Anti-cis to syn-cis TS	23.63	21.5
Syn-cis	0.67	1.1
Syn-cis to syn-trans TS	9.70	9.0
Syn-trans	2.41	2.7
Syn-trans to anti-trans TS	23.37	21.3

These relative energies later become important when trying to calculate the rate constants of each reaction as the energy of the transition states are the barriers for each isomerization reaction. When comparing these values with the study that has been run at a different method called CBS-QB3, we see that the values are comparable to those from the literature.[16] The greatest difference of the barrier height to that of the literature was 2 kcal/mol. From the results above, we see that the highest barriers are the transition from

anti to syn conformation. One of our major interests is to determine whether the anti⇌syn conversion is significant under atmospheric conditions.

3.1.2 Rate of reaction and Population distribution

After finding the molecular geometry of the four conformers and their respective transition states, the data have been inputted into MESMER to calculate the rate constants. Overall, the cis⇌trans conversion have much higher rate constants than that of anti⇌syn conversion (**Figure 4**). Compared to conversion between anti⇌syn, cis⇌trans conversion have a lower barrier to their isomerization leading to fast conversion between each other. Because the transition state involves only the rotation of the C-C central bond, the energy required is lower compared to that of the transition state of the anti⇌syn conversion. With the barrier height of about 20 kcal/mol, the anti to syn conversion requires breaking the C=O double bond to go from one conformation to another. Because the barrier height is considerably high, one of our goals was to determine whether there is any communication between the syn and anti-populations on a time scale that is atmospherically relevant. We will discuss this point below.

In our simulations, we derived the initial population distribution of the MACR oxide conformers based on an earlier study computational study conducted by Kuwata et al. To predict these yields, Kuwata's group studied the cycloreversion of the primary ozonide that leads to the production of MACR oxides, aldehydes, and MACR. Their results show a total yield of 0.44 of MACR oxides for the reaction. Out of the 0.44 yield, they observed that 0.18 gets converted into anti-trans, 0.17 gets converted into anti-cis, 0.06 gets converted into syn-cis and 0.03 gets converted to syn-trans.[16]

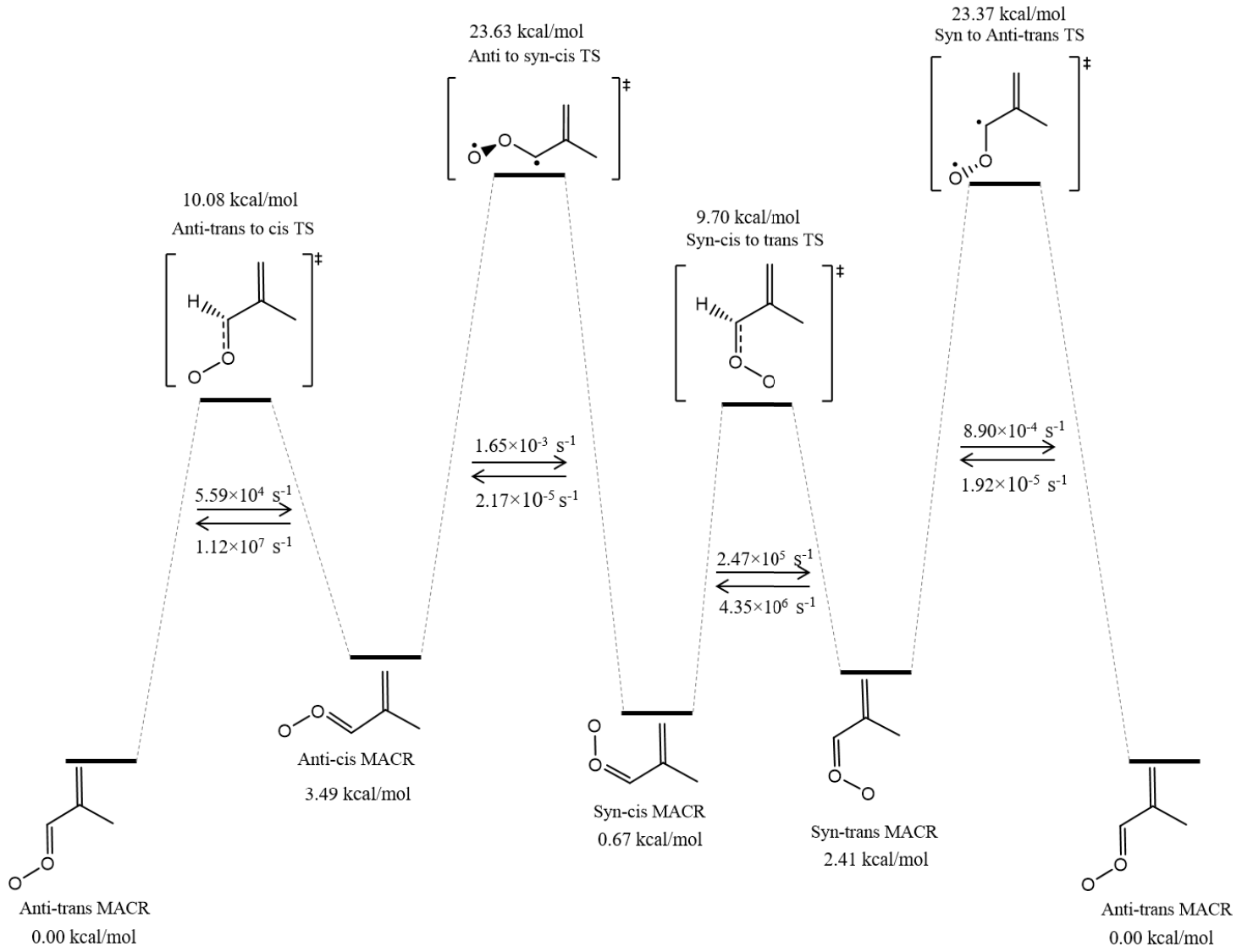

Figure 4. Reaction coordinate of isomerization of MACR oxide with calculated energies and rate constants at 298K and 1 atm Nitrogen. Energies are relative to that of anti-trans MACR.

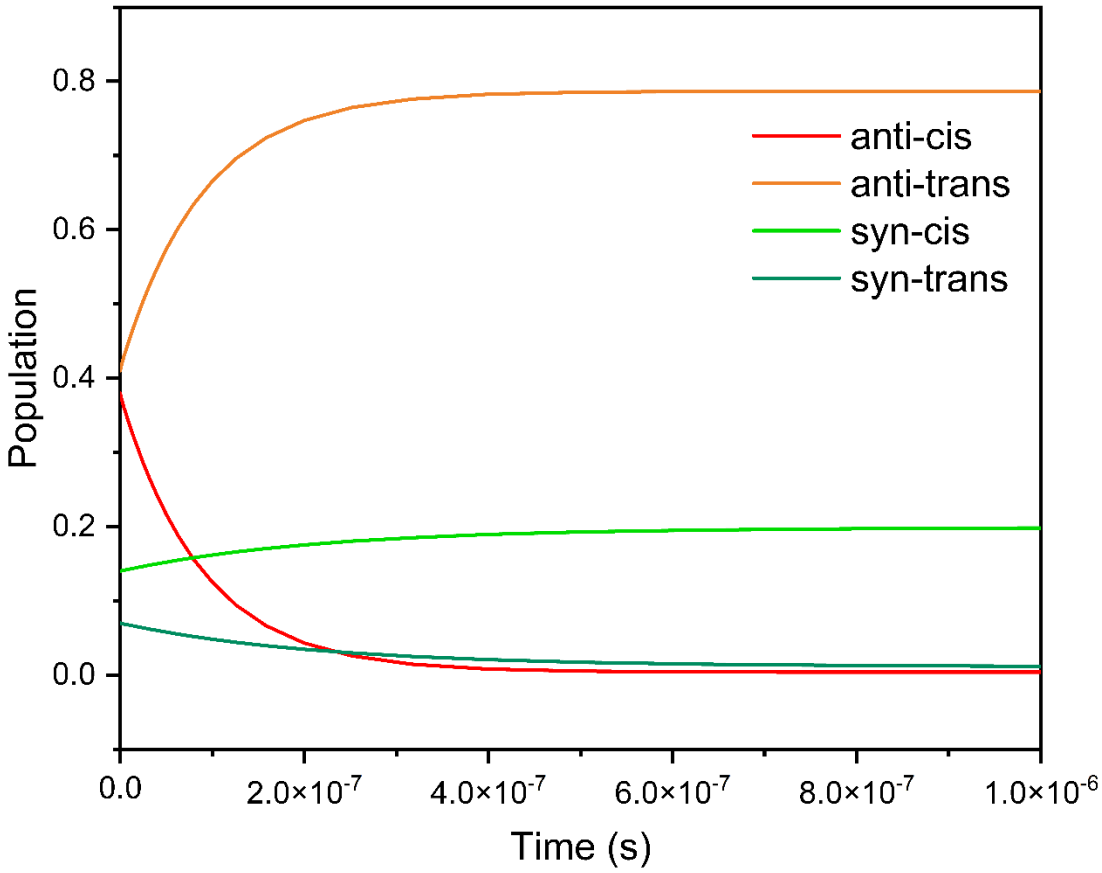

Figure 5. Population distribution of 4 conformers when it has reached quasi-equilibrium.

These ratios then tell us that our reaction should initially start with 41% anti-trans, 38 % anti-cis, 14% syn-cis, and 7% syn-trans in its population. In **Figure 5**, we show how the population distribution of the four conformers evolves in time. After 10 nanoseconds have passed since the reaction has started, we see that isomerization between cis- and trans- conformations is starting. However, we see almost no conversion existing between the syn and anti-conformations. The total amount of anti and syn conformation stays around 80% and 20% respectively even after a microsecond. The same population ratio of anti and syn conformers is maintained until 1 second has passed

indicating that quasi-equilibrium is being established. Currently, the longest lifetime of MACR oxide that has been observed under experimental measurements with atmospheric conditions is 18 ms at 298 K.[25] Because within this timeframe we observe no change in the ratio of anti to syn MACR oxide, we conclude that the anti⇌syn conversion barrier height is too high for this isomerization reaction to having significance under atmospheric conditions.

3.2 Unimolecular Decay Pathways of MACR oxide: Dioxirane and Dioxole Channels

3.2.1 Optimization of Molecular Geometry

Along with the isomerization pathways of MACR oxide, other pathways to lower energy states are available to this Criegee intermediate. Specifically, by going through a ring closure between the carbonyl carbon and the oxygen tail, a new low energy structure is formed called dioxirane. The dioxirane can exist as two conformers, cis and trans.

The cis conformation has the oxygen ring pointed towards the C=C double bond while the trans-dioxirane has the oxygen ring faced away from the C=C double bond. We see that trans-dioxirane has relatively lower energy than that of cis-dioxirane (**Figure 6**). Formation of dioxirane is possible for all four MACR oxide conformers. In **Figure 6**, the transition states for the formation of dioxirane from anti-trans, anti-cis, and syn-trans MACR oxides are shown. Previous work demonstrated that the barrier to the formation of cis-dioxirane from syn-cis-MACR oxide is prohibitively high with a value of 26.4 kcal/mol.[16] In addition, the syn-cis conformation can go through a different ring closure and form a dioxole structure.

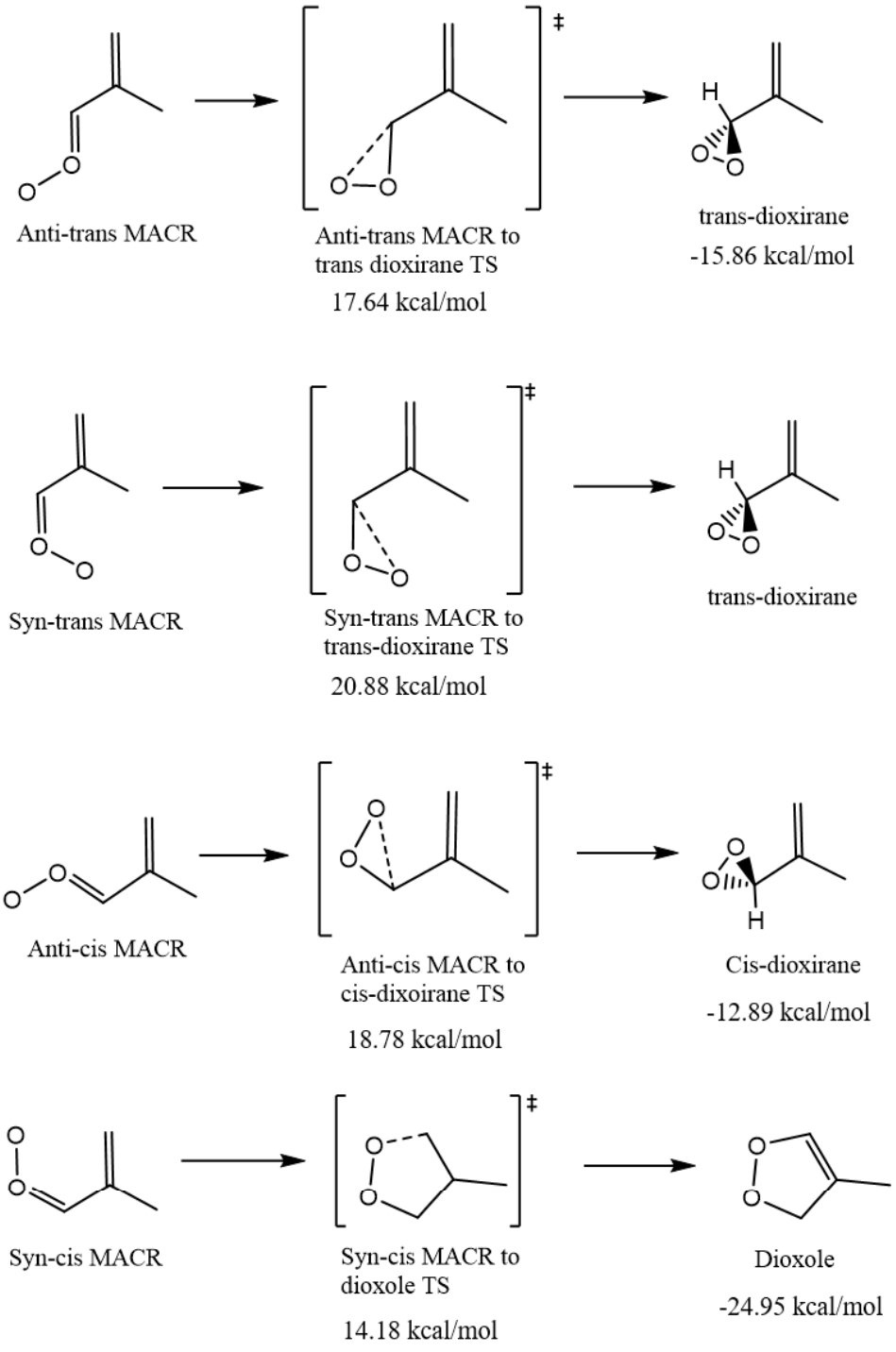

Figure 6. Unimolecular decay pathways of different conformation of MACR oxides. The energies listed are relative to that of the anti-trans MACR oxide.

Table 5. Relative energies of the MACR oxide four conformers and their transition states compared to anti-trans MACR oxide. The energies were calculated using B2PLYPD3/cc-pVTZ.

Type of Structure	Calculated Energy (kcal/mol)	Literature[16] (kcal/mol)
Trans-dioxirane	-15.86	-10.0
Cis-dioxirane	-12.89	-7.1
Dioxole	-24.95	-16.7
Syn-trans to trans-dioxirane TS	20.88	19.0
Anti-trans to trans-dioxirane TS	17.64	16.4
Anti-cis to cis-dioxirane TS	18.78	17.1
Syn-cis to dioxole TS	14.18	13.0

This structure has the most stability out of all the unimolecular decay pathways. Although these ring-closure structures (dioxirane and dioxole) have substantially lower energies than all the MACR oxide conformations, the barriers to achieve the ring closure are moderately high. Our question then became if there is a competition between the isomerization and unimolecular decay pathways and if so, how this competition affects population density under atmospheric conditions.

3.2.2. Rate of reaction and population distribution

Like the four major conformers, once the molecular geometry of the dioxiranes, dioxole, and their respective transition states was calculated, the data was inputted to MESMER to calculate the rate of each reaction. Even after implementing the unimolecular decay reaction, the highest barriers are still that of anti⇌syn conversion of the four major conformers at about 20 kcal/mol.

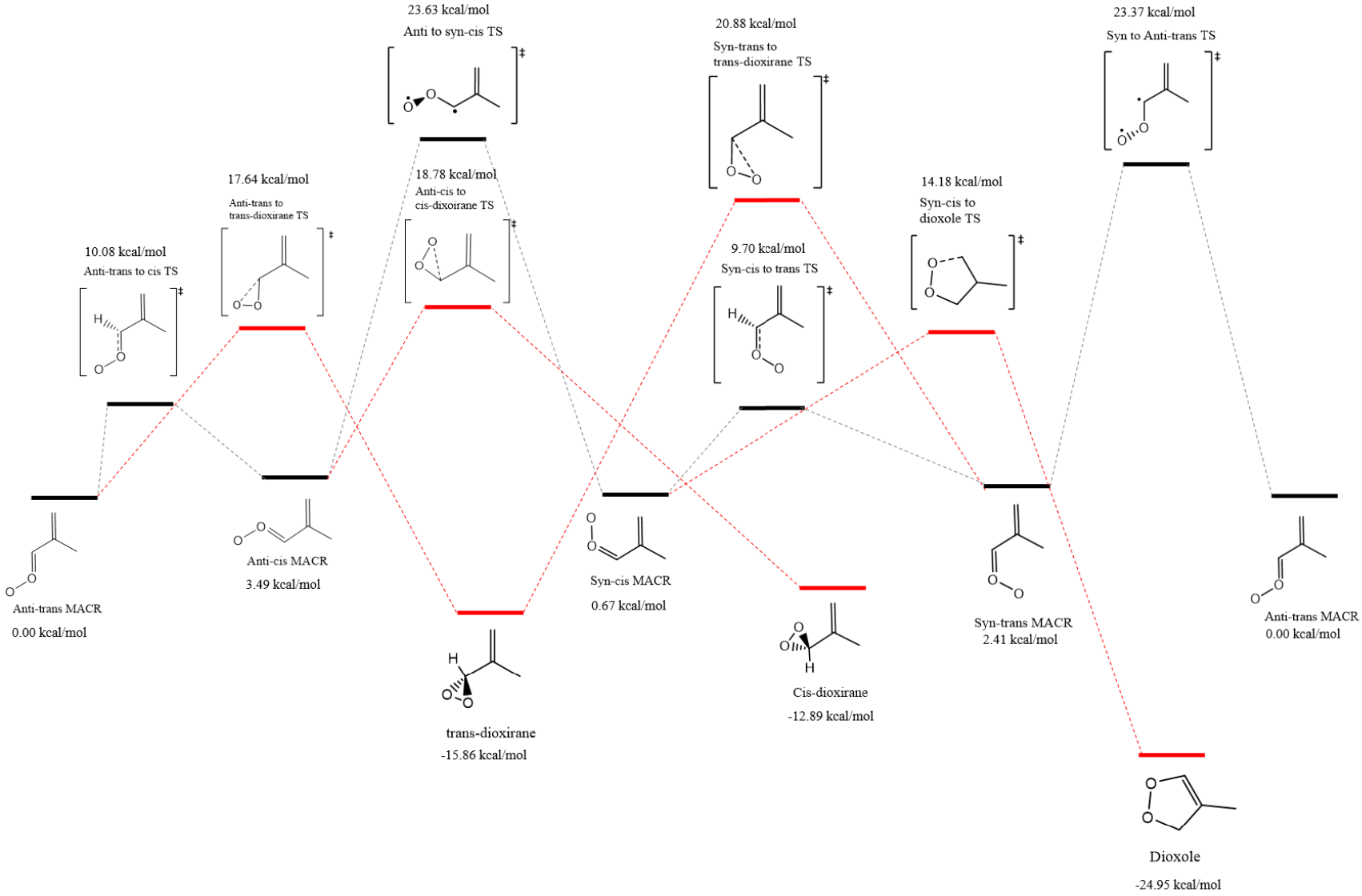

Figure 7. Reaction coordinate of MACR oxide isomerization (indicated in black) and unimolecular decay pathways (indicated in red). The energies listed are relative to that of anti-trans MACR oxide.

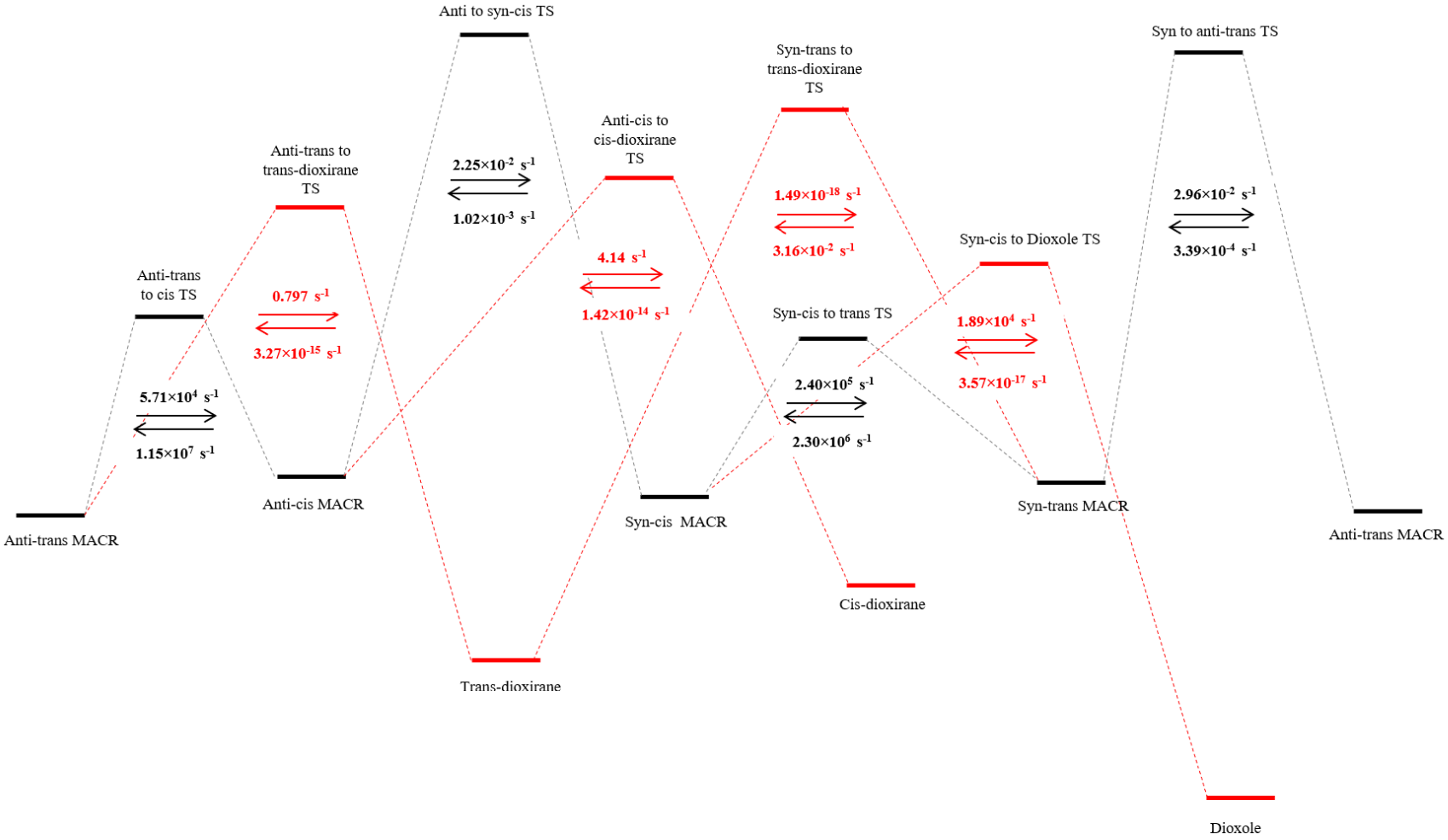

Figure 8. Respective rate constants for the MACR oxide isomerization (indicated in black) and unimolecular decay reactions (indicated in red).

However, the transition states to the dioxiranes and the dioxole are also moderately high in their energy with the barriers ranging from 15-18 kcal/mol (**Figure 7**). Due to the high barrier of the anti⇌syn transitions we see that for the rate constants that are chemically relevant (neglecting the back reactions of the unimolecular reactions since these values are really low and not atmospherically relevant) are still the lowest with values of about 2×10^{-2} s^{-1} (**Figure 8**).

Of all the unimolecular reactions forming dioxirane structures, we see that the syn-trans MACR oxide to trans-dioxirane reaction has the slowest conversion which is a result of having the highest barrier of about 18 kcal/mol while the anti-trans to trans-dioxirane and anti-cis to cis dioxirane have about 17 kcal/mol and 15 kcal/mol barriers respectively (**Figure 7**). The syn-cis MACR oxide to dioxole reaction happens relatively quickly although not as fast as the trans⇌cis isomerization reactions. This observation is due to the energy barrier being relatively low at 14 kcal/mol compared to other high barriers that exist (**Figure 7**).

To see how the newly calculated rate constants might affect the population distribution in the atmosphere, the population versus time graph was plotted again. On a timescale of much less than one microsecond, we see the isomerization reaction cis⇌ trans starting to move forward. Most of the anti-cis has transformed into a more stable structure of anti-trans MACR oxide while the syn-trans and syn-cis MACR oxide structures have reached their steady-state populations (**Figure 9; panel A**). This pattern was also observed in **Figure 5** when only isomerization reaction pathways were mapped on to the reaction coordinate diagram. Once one microsecond has passed, we see that

syn-cis MACR oxide starts to transform into the most stable conformation available: dioxole. There is a rapid increase in the population of dioxole indicating that there is an efficient conversion between syn-cis MACR oxide and dioxole (**Figure 9; panel B)**. Because of the rapid conversion between syn-trans and syn-cis conformers (**Figure 9; panel A**) on a 500 ns timescale, the formation of dioxole efficiently depletes the population of both syn conformers.

Once 100 microseconds have passed, we see the anti-trans MACR oxide start to decrease in its population and trans-dioxirane start to increase in its population. Cis-dioxirane also starts to increase in its population (**Figure 9; panel C**). The increase in cis-dioxirane population is indicative of conversion between anti-trans and anti-cis. The newly created anti-cis population then decay into its product cis-dioxirane before being able to transform back to anti-trans MACR oxide. The formation of cis-dioxirane from anti-cis consist of lower energy pathway compared to the formation of trans-dioxirane from anti-trans. Thus cis-dioxirane is more heavily represented in the branching at 7 seconds (**Figure 9; panel C**) than might be expected from the earlier steady-state population of the anti-cis conformer.

After 1 second what remains is then the relatively stable structures of the unimolecular reactions: trans-dioxirane, cis-dioxirane, and dioxole (**Figure 9; panel C**). When looking closer at the quasi-equilibrium concentrations of the molecules we can see that dioxole has a population of 0.22. This number matches up with the total population of the syn conformers at the beginning of the reactions indicating that most of the syn conformers have transformed into dioxole. Anti-conformers, on the other hand, have only transformed into dioxiranes.

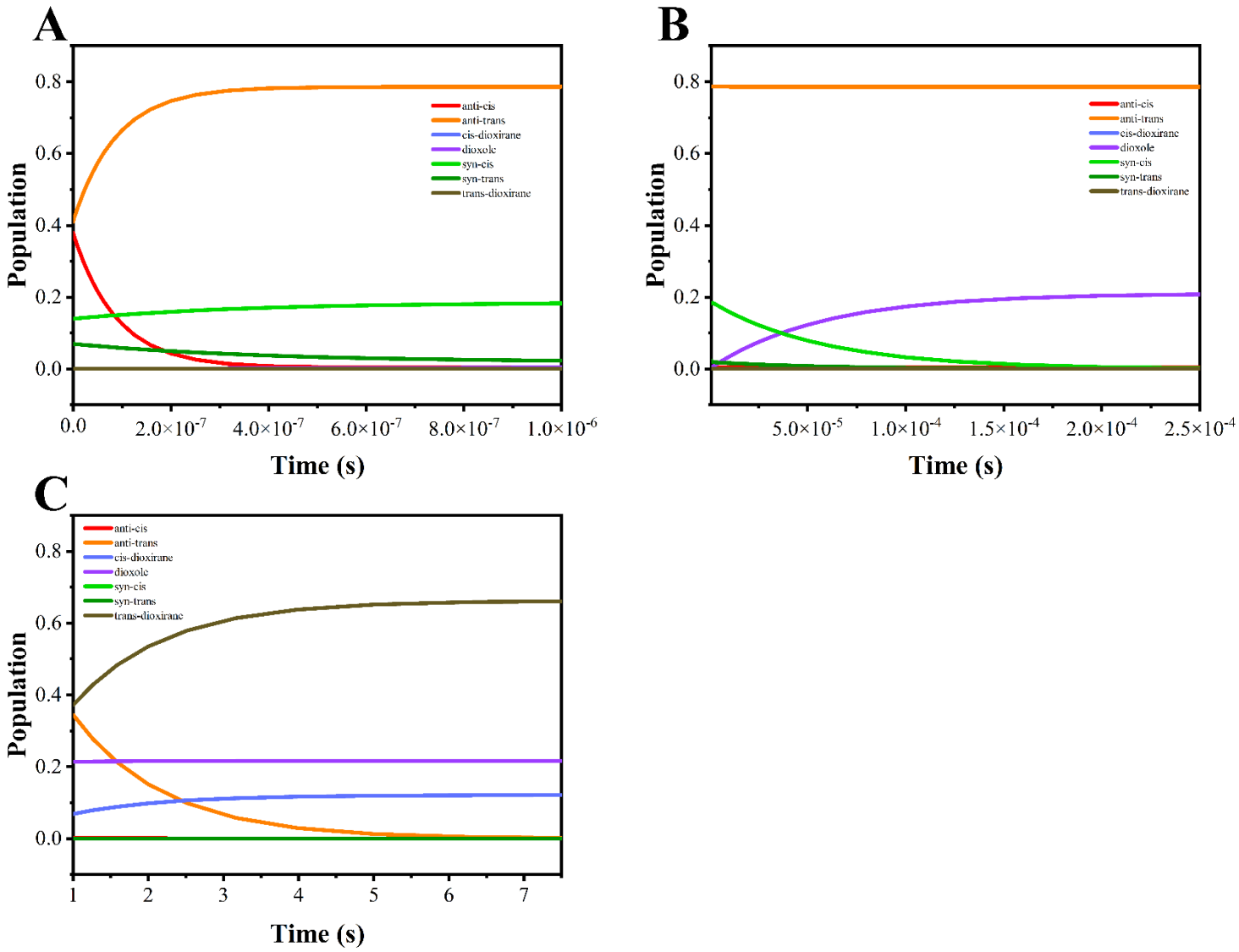

Figure 9. Population distribution of MACR oxide conformations for a) 0-1 μs b) 1-250 μs c) 1-7 s

Table 6. Population distribution of each conformation when it has reached quasi-equilibrium at 10 secs.

Structure	Population
Anti-cis MACR oxide	1.0×10^{-6}
Anti-trans MACR oxide	2.0×10^{-4}
Cis-dioxirane	0.12
Dioxole	0.22
Syn-cis MACR oxide	1.3×10^{-11}
Syn-trans MACR oxide	1.4×10^{-12}
Trans-dioxirane	0.66

The final population of the dioxiranes is 0.78 which matches closely to the anti-conformer population we started with (**Table 6**). Seeing that there was almost no change in the ratio of anti and syn conformers, in the end, indicates to us that there is no conversion of anti⇌syn conformations of MACR oxides. Although dioxole provides the most stable energy conformation out of all the structures, the anti and syn-transformation barrier is simply too high for the anti-molecules to leak into the syn population.

From the previous isomerization reaction of the MACR oxide, we have learned that in atmospheric conditions that anti and syn conversion can be considered negligible as the conversion takes place in a period that is longer than the lifetime of MACR oxide. We see a similar pattern emerging again even when the unimolecular decay reactions have been included in MESMER. Realistically, we can say that some of the long-term behaviors of MACR oxides are not relevant as they would be unobservable on timescales that are atmospherically relevant. We conclude that under the conditions examined (P = 1

atmosphere, T = 298 K), only the cis-trans isomerization and the unimolecular decay of the syn-conformers to the dioxole occur on a timescale that is short enough (10- 20 milliseconds[25]) to be atmospherically relevant. Although we see interesting behavior regarding the formation of dioxirane structures at longer times, we can safely conclude that these unimolecular reactions do have a significant atmospheric impact.

3.3 Effects of Tunneling and Temperature on Rate Constants

For the reactions above, tunneling has not been factored into the calculation of the rate constants. Because the reaction coordinates involved exclusively heavy atoms, we predicted that including tunneling in our calculations would not have significant effects on the rate constants of the reactions of interest. Also, unlike other Criegee intermediates with alkyl substituents on the carbonyl, MACR oxide cannot go through a 1,4-hydrogen transfer mechanism for its decay leading us to infer that tunneling may be negligible for its reactions.

To test if this assumption is true, we have accounted for tunneling into our MESMER calculations and compared the values to those with no tunneling. We see that for the first four reactions in **Table 7**, there is not a substantial amount of change in the rate constant with only about 0.5 to 3 percent chance. The reason why there is a negligible effect of tunneling is that these reactions have the smallest imaginary frequency indicating that the reaction coordinate is dominated by the motion of the heavy atoms. Since tunneling is ineffective with heavy atoms, we see almost no change. Meanwhile, the unimolecular decay reactions experience a significantly larger change in their rate constants (**Table 7**). These reactions have higher frequency motions to get over the barrier. The ring closure reactions involve some H atom motion coupled with heavy

atom motion such that it allows tunneling to have a greater impact. The results then show us that for certain reactions we should worry about how tunneling might affect the reaction rates.

Another factor to be considered is temperature. The average temperature of the surface of the Earth is reported to be 288 K.[26] Because our reactions were run at 298 K, it was important to see if decreasing the temperature to a more atmospherically relevant temperature resulted in any change in the reaction rate.

Table 7. Rate constants of each reaction at no tunneling and tunneling conditions and their respective percent changes. The respective reverse reactions show the same percentage change in the rate constants.

Reactions	Rate constants No Tunneling (s^{-1})	Rate constants Tunneling (s^{-1})	Imaginary Frequency (cm^{-1})	Percent Change
anti-cis → anti-trans	1.12×10^{7}	1.15×10^{7}	160	2.57
syn-trans → syn-cis	1.45×10^{6}	1.46×10^{6}	104	0.74
syn-trans → anti-trans	2.00×10^{-2}	2.02×10^{-2}	211	0.99
anti-cis →syn-cis	3.45×10^{-2}	3.47×10^{-2}	440	0.58
anti-trans → trans-dioxirane	0.609	0.797	506	30.8
anti-cis → cis-dioxirane	3.21	4.14	500	28.9
syn-trans → trans-dioxirane	1.29×10^{-2}	2.12×10^{-2}	611	63.8
syn-cis → dioxole	4.97×10^{3}	6.28×10^{3}	467	26.4

Table 8. Rate constants for different reaction pathways of MACR oxide at different temperatures.

Reactions	Rate constants 298 K (s^{-1})	Rate constants 288 K (s^{-1})	Percent Decrease
anti-trans → anti-cis	5.56×10^{4}	3.38×10^{4}	39.2
anti-cis → anti-trans	1.12×10^{7}	8.43×10^{6}	24.8
syn-trans → syn-cis	2.28×10^{6}	1.58×10^{6}	30.8
syn-cis → syn-trans	2.38×10^{5}	1.52×10^{5}	36.3
anti-trans → syn-trans	3.42×10^{-4}	1.19×10^{-4}	65.0
anti-cis → syn-cis	2.28×10^{-2}	9.69×10^{-3}	57.5
anti-trans → trans-dioxirane	0.609	0.212	65.2
anti-cis → cis-dioxirane	3.21	1.28	60.2
syn-trans → trans-dioxirane	1.89×10^{-2}	7.21×10^{-3}	61.9
syn-cis → dioxole	1.49×10^{4}	8.01×10^{3}	46.4

Overall, the rate constants decreased about 40% for all the reactions at 288 K (**Table 8)**. This observation makes sense as all of the reactions studied have substantial reaction barriers. As expected the reactions with the largest barrier have the largest sensitivity to the temperature. We can therefore conclude that the use of atmospherically relevant temperature does not lead to any changes in the conclusion drawn.

Chapter 4: Conclusion and Future Directions

Criegee intermediates are an important part of atmospheric chemistry. As mentioned in the previous sections, because Criegee intermediates can become a source of OH radicals, it is essential to know what the fate of the Criegee intermediates is. In part, we were interested in studying one specific Criegee intermediate, MACR oxide. The competition between the isomerization reactions and the unimolecular reactions became the focus of our study. Rate constants for the relevant reactions were calculated by implementing RRKM theory and using Master Equation modeling to create a scheme for the system. The rate constant calculations are sensitive to how accurate the molecular geometry of each structure is as this factor affects the RRKM calculations. The calculation is also sensitive to temperature and tunneling factors, so it is important to include those in our calculations.

The overall results show that the most favorable reaction of MACR oxide is the isomerization between the cis and trans conformations. Because the transition states between these conformations are relatively low compared to the other transition states in the reaction, the conversions are observed to happen at a faster rate than the others. The next fastest reaction that takes place was the unimolecular decay reactions to the dioxiranes and the dioxole. However, it was found that the substantial amount (80%) of MACR oxide cannot transform to the most stable structure of dioxole in an atmospherically relevant time frame as the barrier for the conversion between anti and syn is too high. We saw that there was almost no communication between the anti and syn conformers in any of our calculations.

Adding in tunneling to the reaction pathway did not result in an overall change in the pattern mentioned in the previous paragraph. However, some of the reactions did experience some change in the values of their reaction's constants. The unimolecular decay reactions were most affected by the addition of tunneling while the other reactions did not see much of an effect. Adding in temperature to our calculations resulted in a decrease in all the reaction rates. This outcome was expected as by lowering the temperature the number of collisions that the molecules go through with the bath gas decreases leading to a harder time for the molecules to achieve the energy needed to go over the barrier of the reactions.

Because we now have results for what is happening in the standard conditions and some idea of how temperature and tunneling affect the reactions, it is important to have a further understanding of what happens in atmospherically relevant temperatures. Of particular interest is how the reaction rates might be affected by different temperatures. Our atmosphere has different temperatures for each specific layer and depending on the temperature there may be a chance that the rate constants of the isomerization and unimolecular decay reactions might change. However, it is also possible that pressure or even both pressure and temperature could lead to potential communication between the anti and syn population. It is also possible that at certain temperatures, the conversion to dioxiranes and the dioxole could also not happen during the lifetime of the MACR oxide.

Another interesting factor to investigate is how might interaction with different atmospheric molecules affect the different reaction pathways. Our atmosphere does not simply contain only nitrogen gas but also other molecules such as water, O_2, SO_2, and NO_x.[1] It is therefore important to see not only the competition between the isomerization

reaction and the unimolecular decay reaction but also how might biomolecular reactions with these molecules affect the MACR oxide and its reaction pathways.

References

(1) Stephenson, T. A.; Lester, M. I. Unimolecular Decay Dynamics of Criegee Intermediates: Energy-Resolved Rates, Thermal Rates, and Their Atmospheric Impact. *International Reviews in Physical Chemistry* **2020**, *39* (1), 1–33. https://doi.org/10.1080/0144235X.2020.1688530.

(2) Sindelarova, K.; Granier, C.; Bouarar, I.; Guenther, A.; Tilmes, S.; Stavrakou, T.; Müller, J.-F.; Kuhn, U.; Stefani, P.; Knorr, W. Global Data Set of Biogenic VOC Emissions Calculated by the MEGAN Model over the Last 30 Years. *Atmos. Chem. Phys.* **2014**, *14* (17), 9317–9341. https://doi.org/10.5194/acp-14-9317-2014.

(3) Vansco, M. F.; Marchetti, B.; Trongsiriwat, N.; Bhagde, T.; Wang, G.; Walsh, P. J.; Klippenstein, S. J.; Lester, M. I. Synthesis, Electronic Spectroscopy, and Photochemistry of Methacrolein Oxide: A Four-Carbon Unsaturated Criegee Intermediate from Isoprene Ozonolysis. *J. Am. Chem. Soc.* **2019**, *141* (38), 15058–15069. https://doi.org/10.1021/jacs.9b05193.

(4) Zhang, D.; Zhang, R. Mechanism of OH Formation from Ozonolysis of Isoprene: A Quantum-Chemical Study. *J. Am. Chem. Soc.* **2002**, *124* (11), 2692–2703. https://doi.org/10.1021/ja011518l.

(5) Emmerson, K. M.; Carslaw, N.; Carslaw, D. C.; Lee, J. D.; McFiggans, G.; Bloss, W. J.; Gravestock, T.; Heard, D. E.; Hopkins, J.; Ingham, T.; Pilling, M. J.; Smith, S. C.; Jacob, M.; Monks, P. S. Free Radical Modelling Studies during the UK TORCH Campaign in Summer 2003. *Atmos. Chem. Phys.* **2007**, 15.

(6) Emmerson, K. M.; Carslaw, N. Night-Time Radical Chemistry during the TORCH Campaign. *Atmospheric Environment* **2009**, *43* (20), 3220–3226. https://doi.org/10.1016/j.atmosenv.2009.03.042.

(7) Criegee, R. Mechanism of Ozonolysis. *Angew. Chem. Int. Ed. Engl.* **1975**, *14* (11), 745–752. https://doi.org/10.1002/anie.197507451.

(8) Kuwata, K. T.; Hermes, M. R.; Carlson, M. J.; Zogg, C. K. Computational Studies of the Isomerization and Hydration Reactions of Acetaldehyde Oxide and Methyl Vinyl Carbonyl Oxide. *J. Phys. Chem. A* **2010**, *114* (34), 9192–9204. https://doi.org/10.1021/jp105358v.

(9) Vereecken, L.; Harder, H.; Novelli, A. The Reaction of Criegee Intermediates with NO, RO2, and SO2, and Their Fate in the Atmosphere. *Phys. Chem. Chem. Phys.* **2012**, *14* (42), 14682. https://doi.org/10.1039/c2cp42300f.

(10) Lester, M. I.; Klippenstein, S. J. Unimolecular Decay of Criegee Intermediates to OH Radical Products: Prompt and Thermal Decay Processes. *Acc. Chem. Res.* **2018**, *51* (4), 978–985. https://doi.org/10.1021/acs.accounts.8b00077.

(11) Nguyen, T. B.; Tyndall, G. S.; Crounse, J. D.; Teng, A. P.; Bates, K. H.; Schwantes, R. H.; Coggon, M. M.; Zhang, L.; Feiner, P.; Millller, D. O.; Skog, K. M.; Rivera-Rios, J. C.; Dorris, M.; Olson, K. F.; Koss, A.; Wild, R. J.; Brown, S. S.; Goldstein, A. H.; de Gouw, J. A.; Brune, W. H.; Keutsch, F. N.; Seinfeld, J. H.; Wennberg, P. O. Atmospheric Fates of Criegee Intermediates in the Ozonolysis of Isoprene. *Phys. Chem. Chem. Phys.* **2016**, *18* (15), 10241–10254. https://doi.org/10.1039/C6CP00053C.

(12) Taatjes, C. A.; Meloni, G.; Selby, T. M.; Trevitt, A. J.; Osborn, D. L.; Percival, C. J.; Shallcross, D. E. Direct Observation of the Gas-Phase Criegee Intermediate (CH_2OO). *J. Am. Chem. Soc.* **2008**, *130* (36), 11883–11885. https://doi.org/10.1021/ja804165q.

(13) Welz, O.; Savee, J. D.; Osborn, D. L.; Vasu, S. S.; Percival, C. J.; Shallcross, D. E.; Taatjes, C. A. Direct Kinetic Measurements of Criegee Intermediate (CH2OO) Formed by Reaction of CH2I with O2. *Science* **2012**, *335* (6065), 204–207. https://doi.org/10.1126/science.1213229.

(14) Beames, J. M.; Liu, F.; Lu, L.; Lester, M. I. UV Spectroscopic Characterization of an Alkyl Substituted Criegee Intermediate CH_3CHOO. *The Journal of Chemical Physics* **2013**, *138* (24), 244307. https://doi.org/10.1063/1.4810865.

(15) Taatjes, C. A. Criegee Intermediates: What Direct Production and Detection Can Teach Us About Reactions of Carbonyl Oxides. *Annu. Rev. Phys. Chem.* **2017**, *68* (1), 183–207. https://doi.org/10.1146/annurev-physchem-052516-050739.

(16) Kuwata, K. T.; Valin, L. C. Quantum Chemical and RRKM/Master Equation Studies of Isoprene Ozonolysis: Methacrolein and Methacrolein Oxide. *Chemical Physics Letters* **2008**, *451* (4–6), 186–191. https://doi.org/10.1016/j.cplett.2007.11.092.

(17) Vansco, M. F.; Caravan, R. L.; Zuraski, K.; Winiberg, F. A. F.; Au, K.; Trongsiriwat, N.; Walsh, P. J.; Osborn, D. L.; Percival, C. J.; Khan, M. A. H.; Shallcross, D. E.; Taatjes, C. A.; Lester, M. I. Experimental Evidence of Dioxole Unimolecular Decay Pathway for Isoprene-Derived Criegee Intermediates. *J. Phys. Chem. A* **2020**, *124* (18), 3542–3554. https://doi.org/10.1021/acs.jpca.0c02138.

(18) Steinfeld, J. I.; Francisco, J. S.; Hase, W. L. *Chemical Kinetics and Dynamics*, Second.; Prentice Hall: Upper Saddle River, New Jersey 07458, 1999.

(19) Engel, T.; Reid, P. *Thermodynamics, Statistical Thermodynamics, and Kinetics*, 4th ed.; Pearson: New York, NY, 2019.

(20) Glowacki, D. R.; Liang, C.-H.; Morley, C.; Pilling, M. J.; Robertson, S. H. MESMER: An Open-Source Master Equation Solver for Multi-Energy Well Reactions. *J. Phys. Chem. A* **2012**, *116* (38), 9545–9560. https://doi.org/10.1021/jp3051033.

(21) Osborn, D. L. Reaction Mechanisms on Multiwell Potential Energy Surfaces in Combustion (and Atmospheric) Chemistry. *Annu. Rev. Phys. Chem.* **2017**, *68* (1), 233–260. https://doi.org/10.1146/annurev-physchem-040215-112151.

(22) Smith, C. D.; Karton, A. Kinetics and Thermodynamics of Reactions Involving Criegee Intermediates: An Assessment of Density Functional Theory and Ab Initio Methods Through Comparison with CCSDT(Q)/CBS Data. *J Comput Chem* **2020**, *41* (4), 328–339. https://doi.org/10.1002/jcc.26106.

(23) Grimme, S.; Ehrlich, S.; Goerigk, L. Effect of the Damping Function in Dispersion Corrected Density Functional Theory. *J. Comput. Chem.* **2011**, *32* (7), 1456–1465. https://doi.org/10.1002/jcc.21759.

(24) Grimme, S.; Steinmetz, M. Effects of London Dispersion Correction in Density Functional Theory on the Structures of Organic Molecules in the Gas Phase. *Phys. Chem. Chem. Phys.* **2013**, *15* (38), 16031. https://doi.org/10.1039/c3cp52293h.

(25) Lin, Y.-H.; Yin, C.; Takahashi, K.; Lin, J. J.-M. Surprisingly Long Lifetime of Methacrolein Oxide, an Isoprene Derived Criegee Intermediate, under Humid Conditions. *Commun Chem* **2021**, *4* (1), 12. https://doi.org/10.1038/s42004-021-00451-z.

(26) NASA's Cosmos https://ase.tufts.edu/cosmos/view_chapter.asp?id=21&page=1 (accessed Apr 7, 2021).

Supplemental Information

Table S1. Energy of each MACR isomer relative to anti-trans conformation calculated using different density functional methods. The values were compared to literature data computed through high-level Coupled Cluster Model.

Method	Anti-cis (kcal/mol)	Syn-trans (kcal/mol)	Syn-cis (kcal/mol)
B2PLYP	3.46	2.59	0.83
B2PLYPD3	3.49	2.41	0.67
B3LYP	3.45	2.76	1.38
B3LYPD3	3.49	2.26	1.03
MN12L	4.01	2.09	2.00
CCSD-CBS	3.18	2.50	0.91

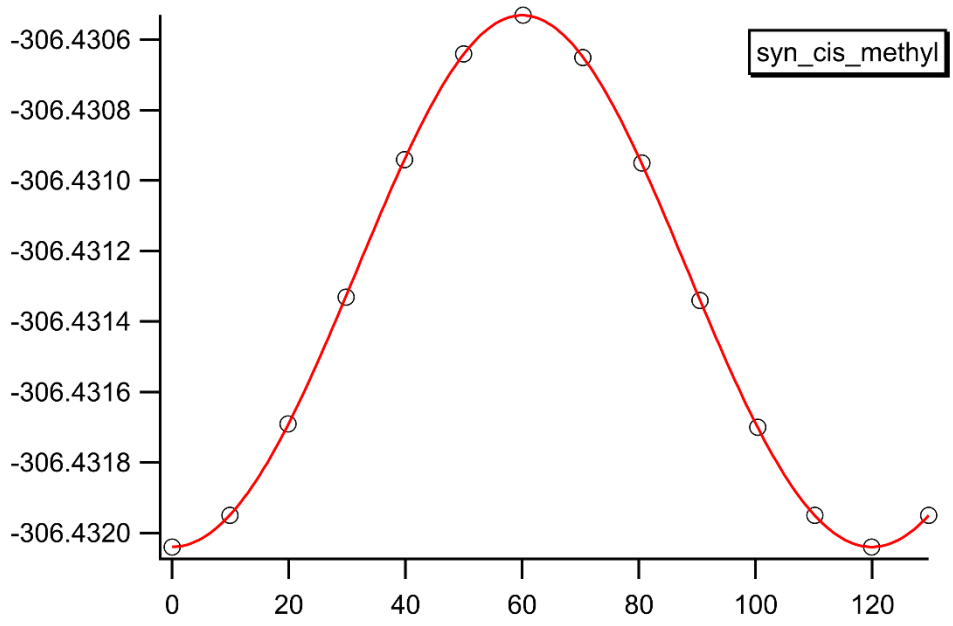

Figure S1. Methyl rotor fit of anti-cis to syn-cis transition state ran under B3LYP calculations. B2PLYPD3 also shows similar result.

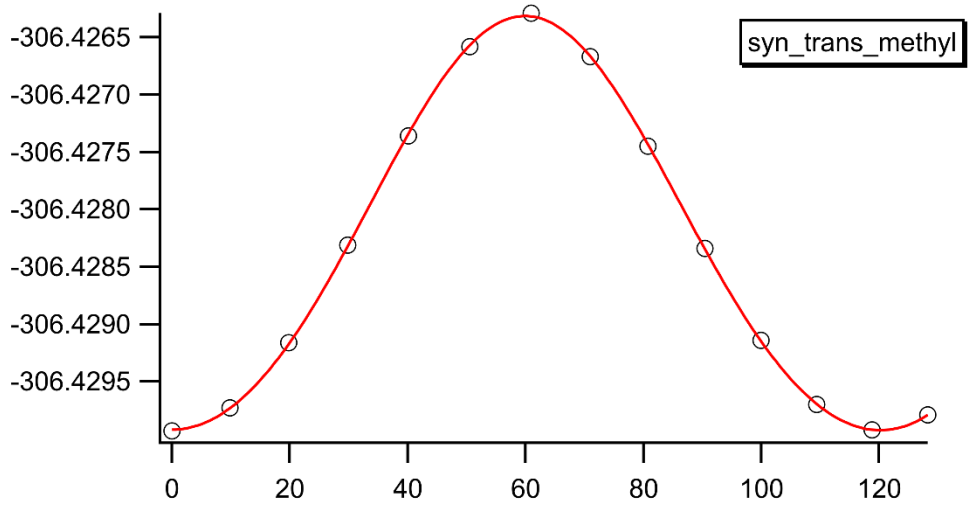

Figure S2. Methyl rotor fit of syn-trans MACR oxide ran under B3LYP calculations. B2PLYPD3 also shows similar result.

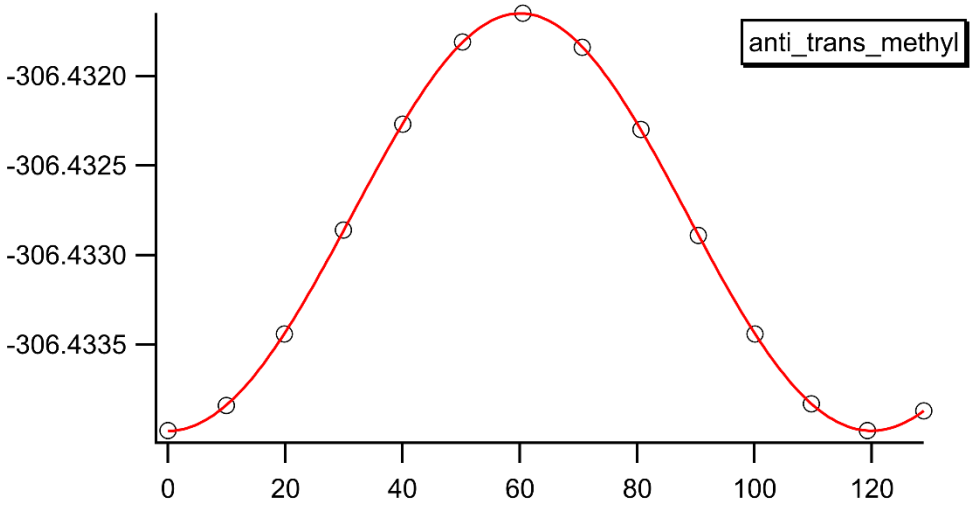

Figure S3. Methyl rotor fit of anti-trans MACR oxide ran under B3LYP calculations. B2PLYPD3 also shows similar results.

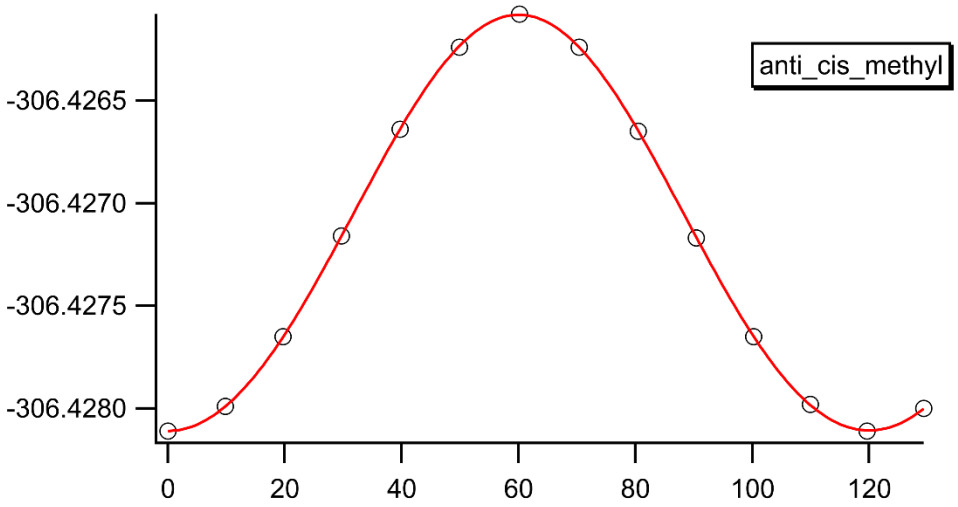

Figure S4. Methyl rotor fit of anti-cis MACR oxide ran under B3LYP calculations. B2PLYPD3 also shows similar result.

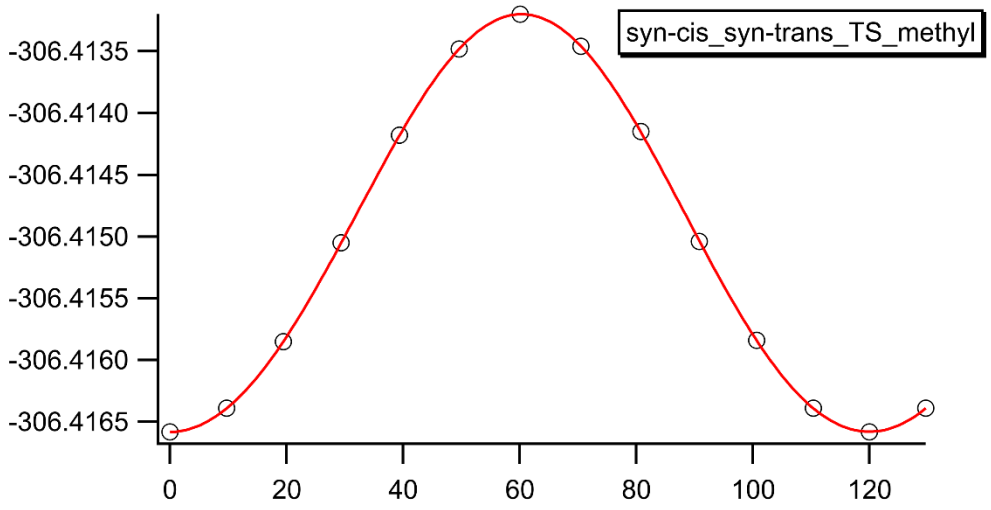

Figure S5. Methyl rotor fit of syn-cis to syn-trans MACR oxide transition state. B2PLYPD3 also shows similar result.

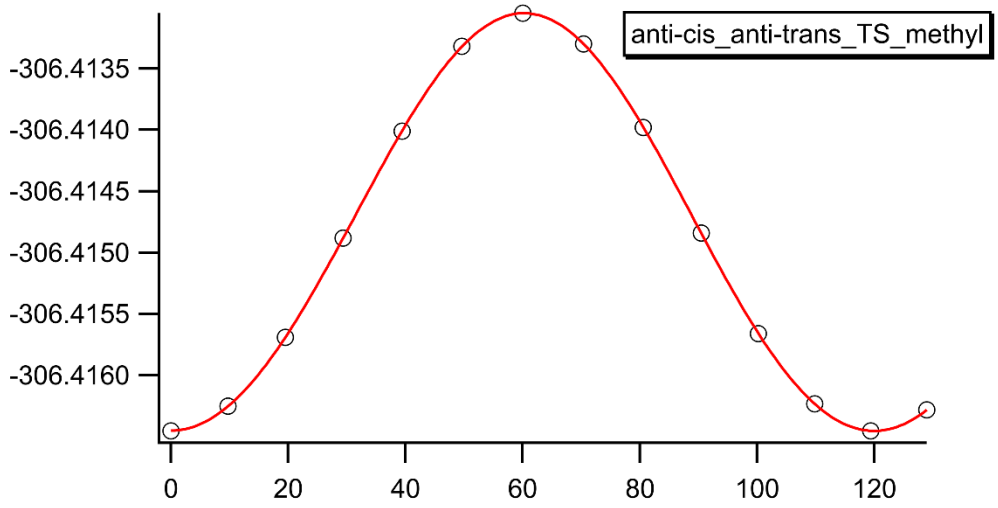

Figure S6. Methyl rotor fit of anti-cis to anti-trans MACR oxide transition state ran under B3LYP calculations. B2PLYPD3 also shows similar result.

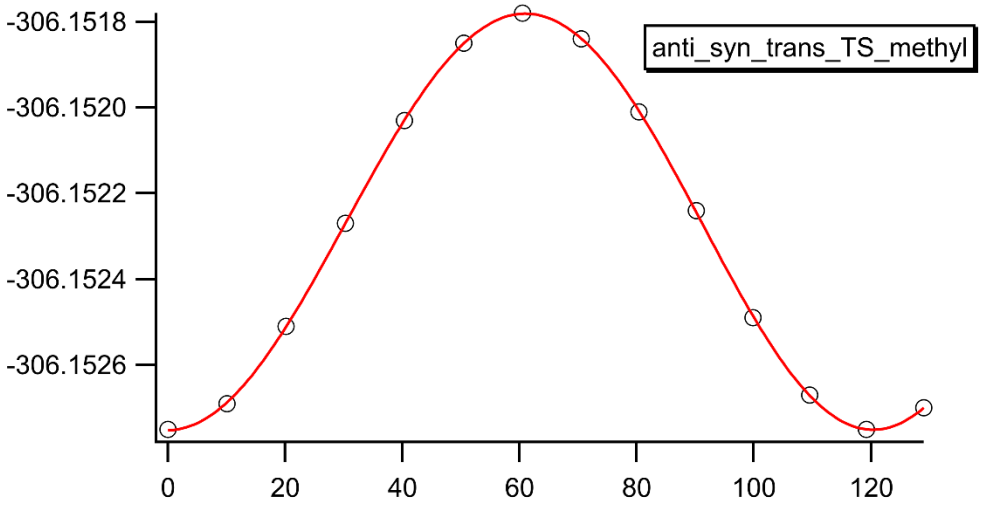

Figure S7. Methyl rotor fit of anti-trans to syn-trans MACR oxide transition state ran under B3LYP calculations. B2PLYPD3 also shows similar result.

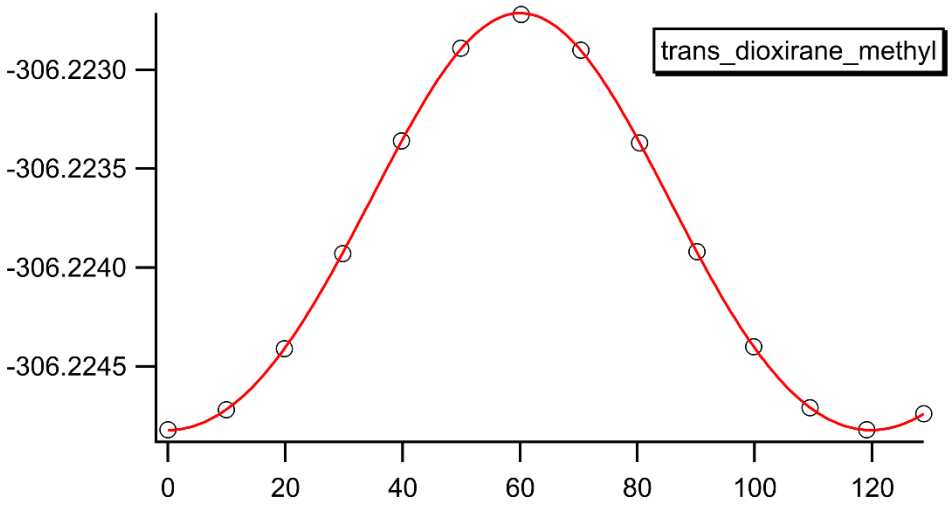

Figure S8. Methyl rotor fit of trans-dioxirane ran under B3LYP calculations. B2PLYPD3 also shows similar result.

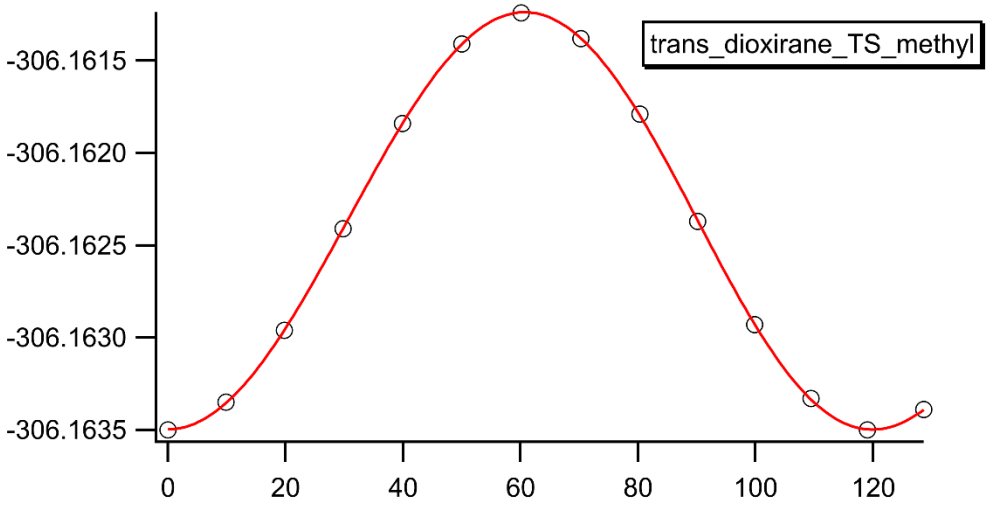

Figure S9. Methyl rotor fit of anti-trans/syn-trans to trans-dioxirane transition state. B2PLYPD3 also shows similar result.

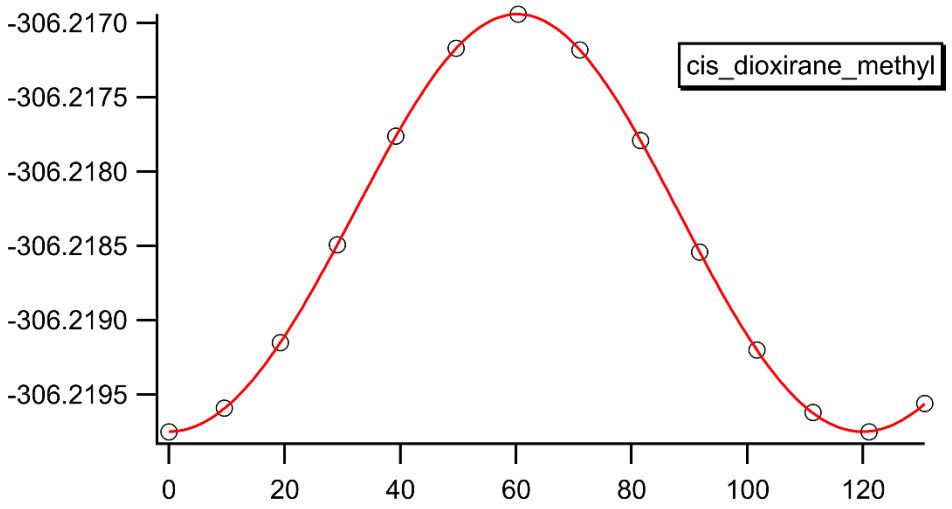

Figure S10. Methyl rotor fit of cis-dioxirane ran under B3LYP calculations. B2PLYPD3 also shows similar result.

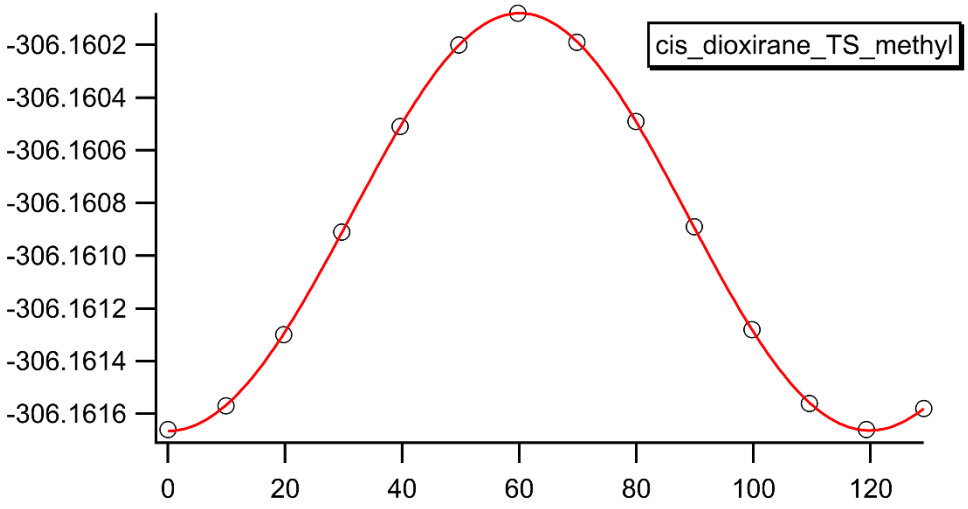

Figure S11. Methyl rotor fit of anti-cis MACR oxide to cis-dioxirane transition state ran under B3LYP calculations. B2PLYPD3 also shows similar result.

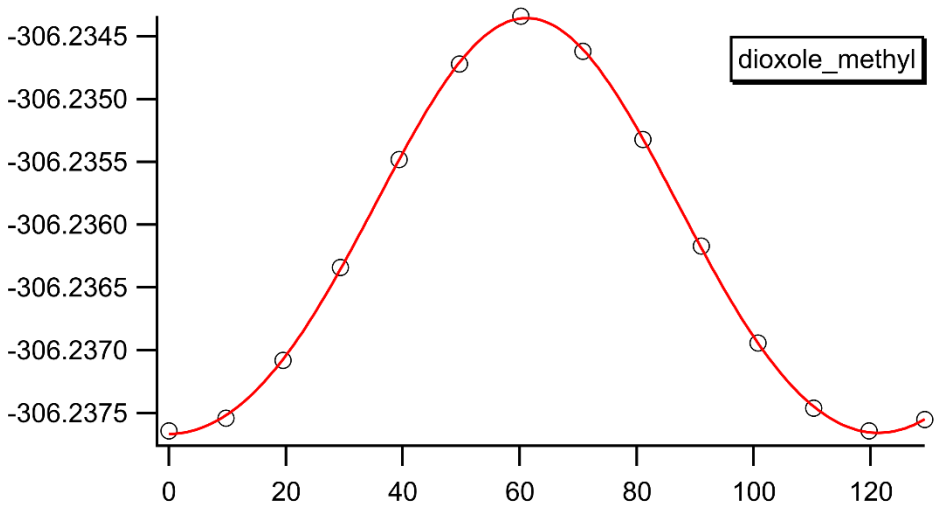

Figure S12. Methyl rotor fit of dioxole ran under B3LYP calculations. B2PLYPD3 also shows similar result.

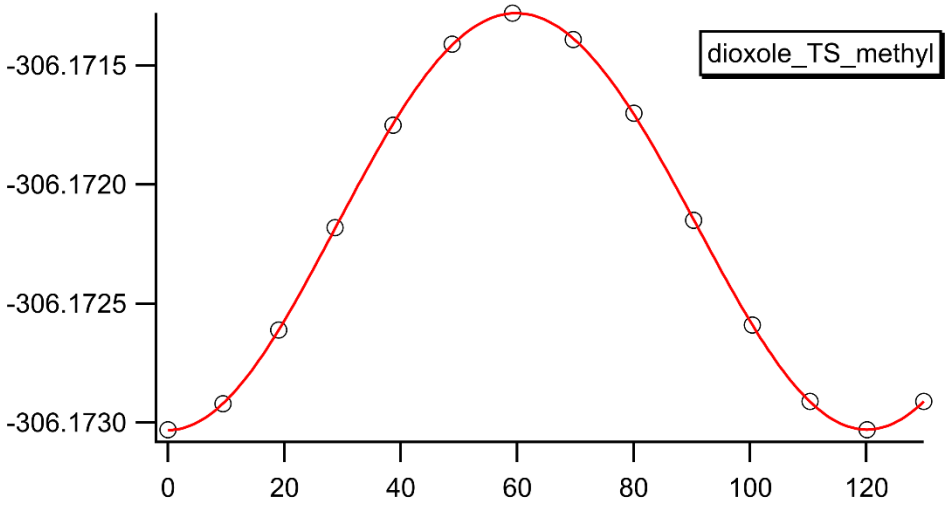

Figure S13. Methyl rotor fit of syn-cis MACR oxide to dioxole transition state ran under B3LYP calculations. B2PLYPD3 also shows similar result.

Table S2. Table of expansion coefficients for methyl hindered potential fit from Igor.

Structures	b_0	b_1	b_2	b_3	b_4	b_5	b_6	b_7	b_8
Anti-trans	-306.1886	6.1827×10^{-5}	-5.3769×10^{-5}	-0.001228	-2.4624×10^{-5}	1.1352×10^{-5}	3.0598×10^{-5}	--	--
Anti-cis	-306.1859	-4.1233×10^{-5}	3.3997×10^{-5}	-0.001118	1.5068×10^{-5}	-6.2172×10^{-5}	3.7448×10^{-5}	--	--
Anti-trans to anti-cis TS	-306.1743	8.3837×10^{-5}	-8.8476×10^{-5}	-0.001730	-2.8766×10^{-5}	3.3810×10^{-5}	2.2677×10^{-5}	--	--
Syn-trans	-306.1874	-0.0004950	0.0004248	-0.002301	0.0002161	-0.0001246	0.0002194	--	--
Syn-cis	-306.4313	-2.076×10^{-5}	2.4713×10^{-5}	-0.0007675	3.0446×10^{-6}	-6.5681×10^{-6}	2.6243×10^{-5}	--	--
Syn-trans to syn-cis TS	-306.4150	-1.6623×10^{-5}	-1.2094×10^{-5}	-0.001699	8.1814×10^{-6}	-3.6737×10^{-5}	7.2465×10^{-5}	--	--
Anti-trans to syn-trans TS	-306.1523	0.00010718	-0.00010755	-0.00040777	-4.4582×10^{-5}	3.8091×10^{-5}	-2.1365×10^{-5}	7.4235×10^{-5}	-1.7193×10^{-5}

Structure	b_0	b_1	b_2	b_3	b_4	b_5	b_6	b_7	b_8
Anti-cis to syn-cis TS	-306.1555	0.00029838	-0.00018214	0.00020134	-0.0002225	0.00010297	7.8024×10^{-5}	2.8231×10^{-5}	-1.6248×10^{-5}
Trans-dioxirane	-306.2239	2.5077×10^{-5}	-2.1335×10^{-5}	-0.0010379	$-1;2182\times10^{-5}$	8.5119×10^{-6}	6.9338×10^{-5}	--	--
Anti-trans to trans-dioxirane	-306.1624	0.00013988	-0.00013367	-0.00103745	-5.0774×10^{-5}	4.4998×10^{-5}	-1.0675×10^{-5}	--	--
Syn-trans to trans-dioxirane	-306.1608	7.83×10^{-6}	6.16×10^{-5}	-0.00116	-6.43×10^{-5}	-2.69×10^{-5}	6.8×10^{-5}	--	--

Table S3. Table of expansion coefficients for methyl hindered potential fit from Igor.

Structures	b_0	b_1	b_2	b_3	b_4	b_5	b_6
Cis-dioxirane	-306.2184	7.6358×10^{-5}	-6.9877×10^{-5}	-0.0013545	-2.9301×10^{-5}	2.3435×10^{-5}	2.867×10^{-5}
Anti-cis to cis-dioxirane	-306.1608	2.0143×10^{-5}	-1.8574×10^{-5}	-0.0007779	-9.8022×10^{-6}	7.1928×10^{-6}	1.0400×10^{-5}
Dioxole	-306.2361	4.1606×10^{-5}	-0.0001083	-0.001615	3.7264×10^{-5}	2.1908×10^{-5}	9.9762×10^{-5}
Syn-cis to dioxole TS	-306.1721	-7.1392×10^{-6}	8.3166×10^{-5}	-0.0008808	3.0686×10^{-6}	-5.6236×10^{-6}	-1.1189×10^{-5}

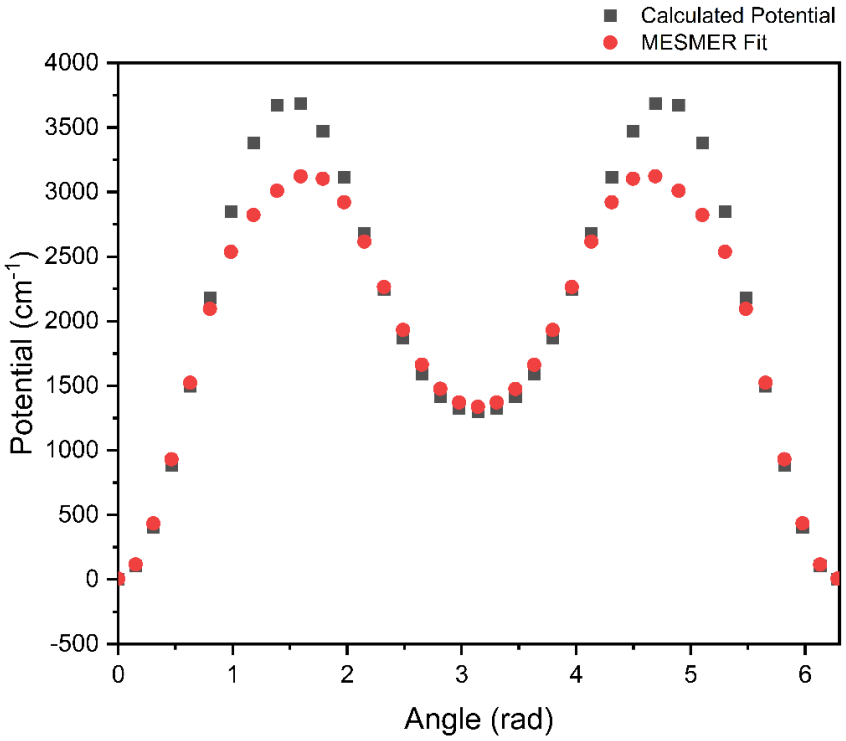

Figure S14. Graph of the calculated potential of anti-trans MACR oxide vs. Mesmer fit. B2PLYPD2 basis set used.

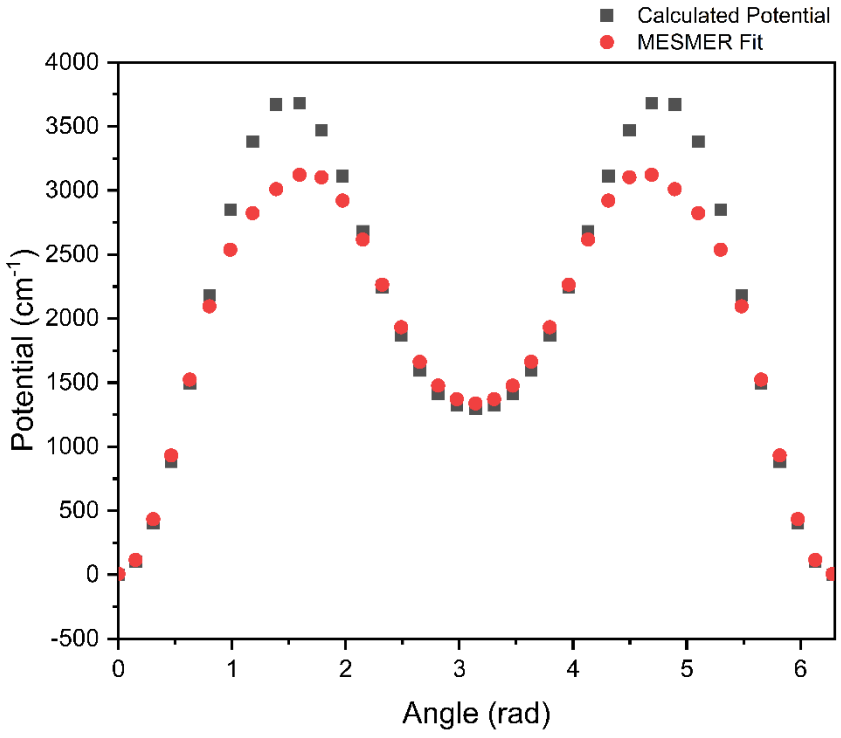

Figure S15. Graph of calculated potential of anti-cis MACR oxide vs. Mesmer fit. B2PLYPD2 basis set used.

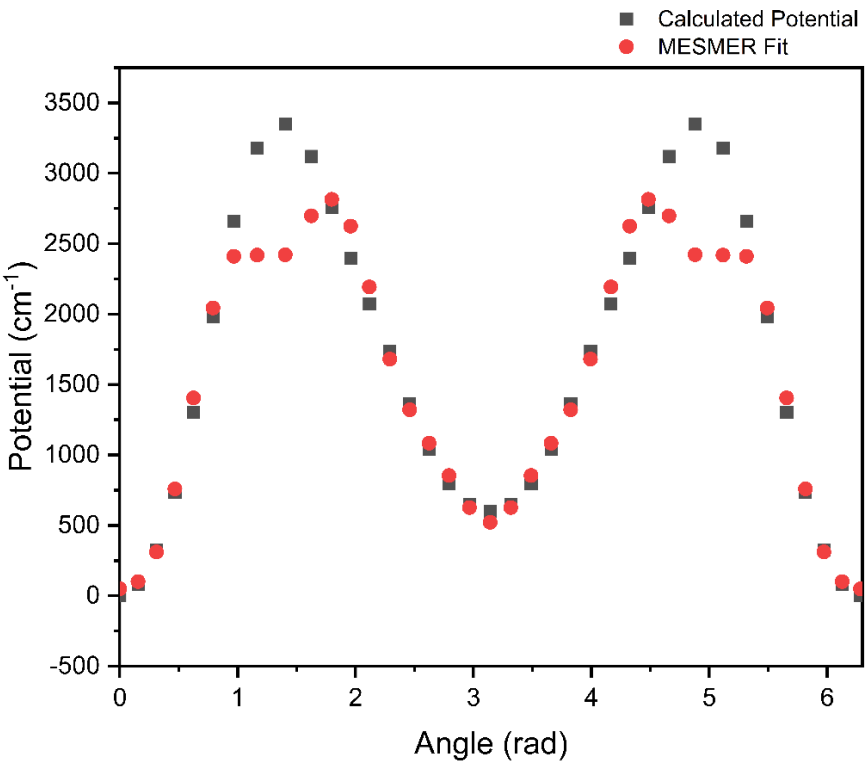

Figure S16. Graph of calculated potential of syn-trans MACR oxide vs. Mesmer fit. B2PLYPD2 basis set used

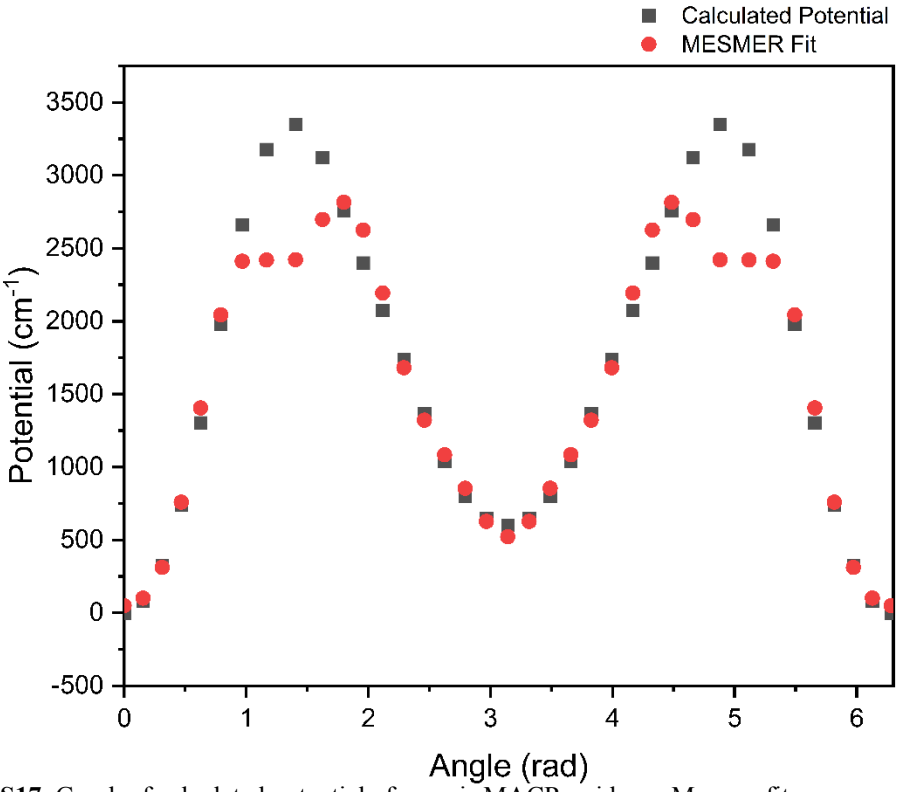

Figure S17. Graph of calculated potential of syn-cis MACR oxide vs. Mesmer fit.

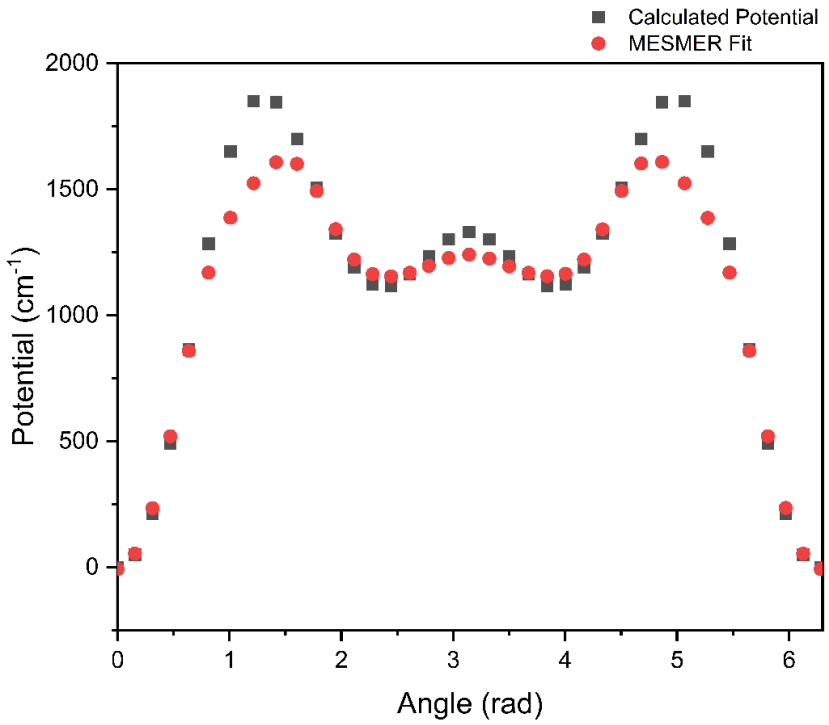

Figure S18. Graph of calculated potential of trans-dioxirane vs. Mesmer fit. B2PLYPD2 basis set used.

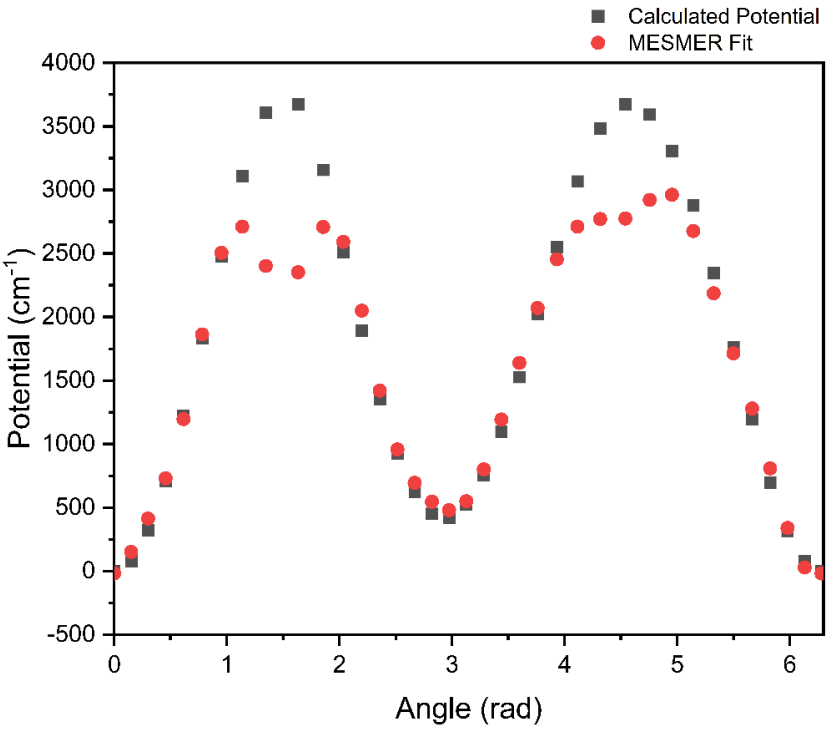

Figure S19. Graph of calculated potential of anti-trans to trans-dioxirane TS vs. Mesmer fit. B2PLYPD2 basis set used.

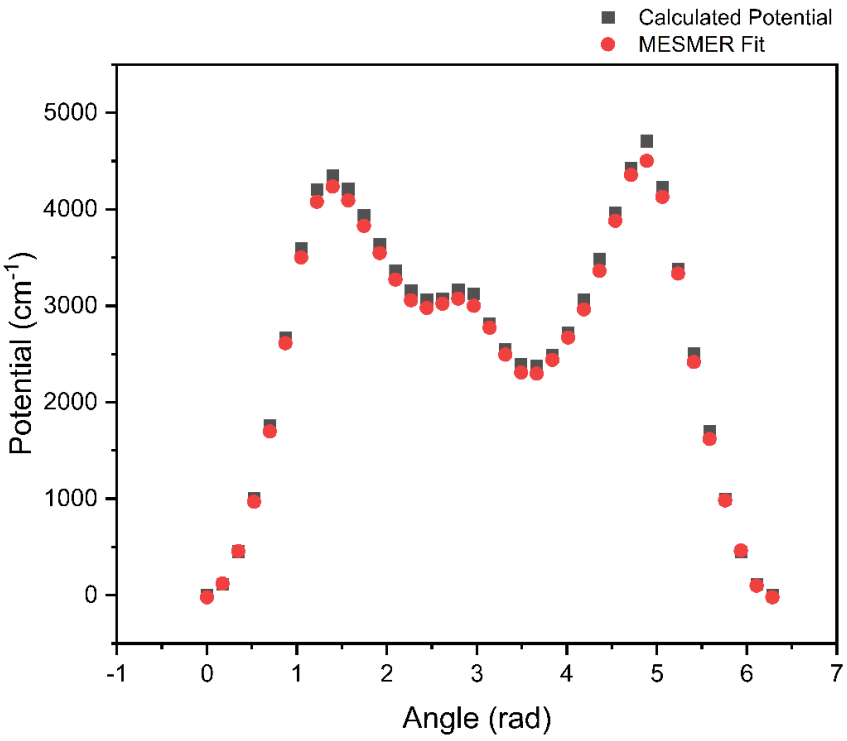

Figure S20. Graph of calculated potential of syn-trans to trans-dioxirane TS vs. Mesmer fit. B2PLYPD2 basis set used.

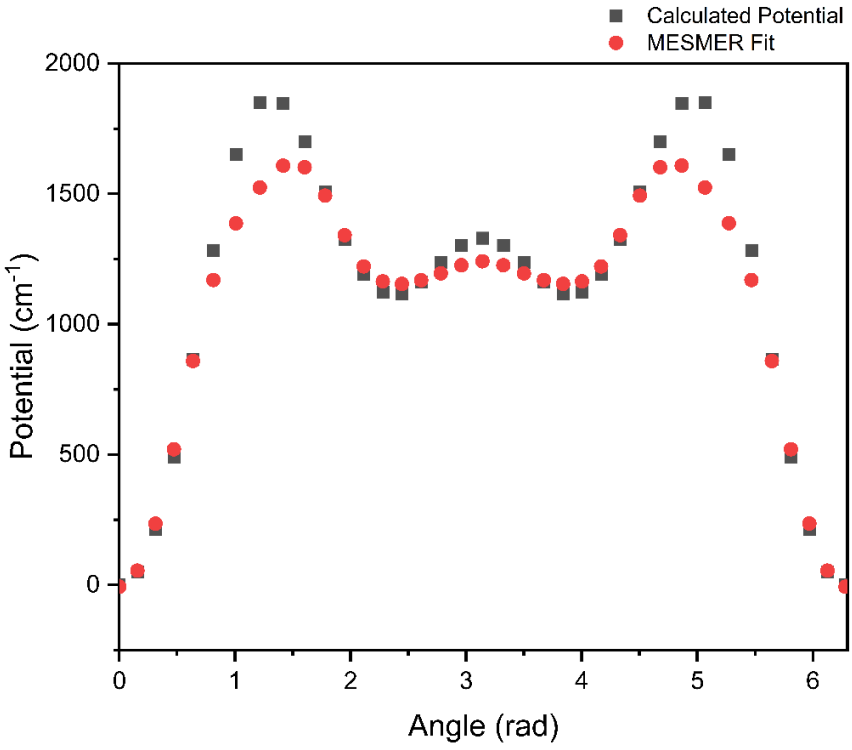

Figure S21. Graph of calculated potential of cis-dioxirane vs. Mesmer fit. B2PLYPD2 basis set used.

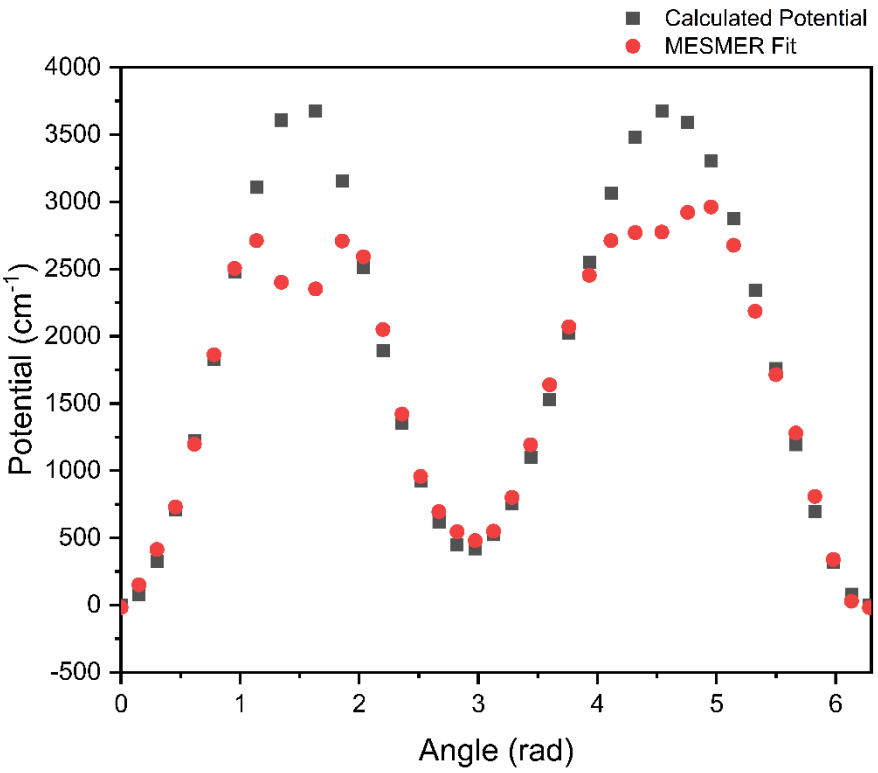

Figure S22. Graph of calculated potential of anti-cis to cis-dioxirane TS vs. Mesmer fit. B2PLYPD2 basis set used.